MISS LUZ ELENA GOMIS-CARTESIO (Orcid ID : 0000-0001-6556-6177)

Article type   : Original Manuscript

Shelf-margin clinothem progradation, degradation and readjustment: Tanqua Depocentre, Karoo Basin (South Africa)

LUZ. E. GOMIS-CARTESIO[1*], MIQUEL POYATOS-MORÉ[1], DAVID M. HODGSON[2] and STEPHEN S. FLINT[1]

[1] *Stratigraphy Group, School of Earth and Environmental Sciences, University of Manchester, M13 9PL, United Kingdom.*

[2] *Stratigraphy Group, School of Earth and Environment, University of Leeds, LS2 9JT, United Kingdom.*

* Corresponding author: luz.gomiscartesio@manchester.ac.uk

Associate Editor – JP Walsh

Short Title – Shelf-margin clinothem degradation and readjustment

ABSTRACT

Degradation of basin-margin clinothems around the shelf-edge rollover zone may lead to the generation of conduits through which gravity flows transport sediment downslope. Many studies from seismic-reflection datasets show these features, but they lack small-scale (centimetre to metre) sedimentary and stratigraphic observations on process interactions. Exhumed basin-margin clinothems in the Tanqua depocentre (Karoo Basin) provide seismic-reflection-scale geometries and internal details of architecture with depositional dip and strike control. At the Geelhoek locality, clinothem parasequences comprise siltstone-rich offshore deposits overlain by heterolithic prodelta

facies and sandstone-dominated deformed mouth bars. Three of these parasequences are truncated by a steep (6 to 22°), 100 m deep and 1.5 km wide asymmetrical composite erosion surface that delineates a shelf-edge canyon. The fill, from base to top comprises: (i) thick-bedded sandstone with intrabasinal clasts and multiple erosion surfaces; (ii) scour-based interbedded sandstone and siltstone with tractional structures; and (iii) inverse-graded to normal-graded siltstone beds. An overlying 55 m thick coarsening-upward parasequence fills the upper section of the canyon and extends across its interfluves. Younger parasequences display progressively shallower gradients during progradation and healing of the local accommodation. The incision surface resulted from initial oversteepening and high sediment supply triggering deformation and collapse at the shelf edge, enhanced by a relative sea-level fall that did not result in subaerial exposure of the shelf edge. Previous work identified an underlying highly incised, sandstone-rich shelf-edge rollover zone across-margin strike, suggesting that there was migration in the zone of shelf-edge to upper slope incision over time. This study provides an unusual example of clinothem degradation and re-adjustment with three-dimensional control in an exhumed basin margin succession. The work demonstrates that large-scale erosion surfaces can develop and migrate due to a combination of factors at the shelf-edge rollover zone, and proposes additional criteria to predict clinothem incision and differential sediment bypass in consistently progradational systems.

Keywords: Clinothem degradation, Karoo basin, sediment bypass, shelf-edge deltas, shelf-margin evolution, submarine canyon.

INTRODUCTION

Basin margin clinothems are fundamental building blocks of continental margin accumulations (e.g. Steel & Olsen, 2002; Helland-Hansen *et al.*, 2012; Patruno *et al.*, 2015). Their development is associated with erosion, transport and accretion of sediment at the basin margin, reflecting the interplay between accommodation and sediment supply. The trajectory of successive clinothem

rollovers is widely employed to interpret and to predict the timing of downslope sediment transfer (Morton & Suter, 1996; Muto & Steel, 2002; Steel & Olsen, 2002; Steel *et al*., 2003; Johannessen & Steel, 2005; Porębski & Steel, 2006; Carvajal & Steel, 2009; Carvajal *et al*., 2009; Covault *et al*., 2009; Olariu & Steel, 2009; Helland-Hansen & Hampson, 2009; Hubbard *et al*., 2010; Dixon *et al*., 2012a; 2012b; Jones *et al*., 2015). However, much less emphasis is placed on phases of significant basin margin degradation that disrupt clinothem stacking patterns (Neal & Abreu, 2009).

Basin margins can be classified according to their graded profile (i.e. long-term equilibrium between depositional and erosional processes; Fig. 1A) and the dominant type and distribution of accommodation (Hedberg, 1970; Ross *et al*., 1994; 1995; Prather *et al*., 1998; Adams & Schlager, 2000; Meckel, 2000; Prather, 2000; 2003; Pyles *et al.*, 2011). Degradation of the shelf-edge rollover zone (SERZ) results in 'out of grade' slopes (Hedberg, 1970; Ross *et al*., 1994; Fig. 1A) and is commonly associated with mass-wasting and sediment bypass. As the slope readjusts, out of grade margins evolve into progradational or graded margins (Hedberg, 1970; Ross *et al*., 1994; 1995; Fig. 1A).

Irregular U-shaped or V-shaped surfaces across the upper slope form large-scale unconformities (e.g. Pratson *et al*., 1994; Pratson & Haxby, 1996; Brothers *et al*., 2013; Fig. 1) that can migrate laterally along basin margins (Kertznus & Kneller, 2009); these can form tens to hundreds of metres deep canyons, channels, and gullies that eventually incise the shelf (e.g., Sanchez *et al*., 2012; Sylvester *et al*., 2012), enhancing the depth of erosion and the onset of gravity-driven density flows and gravitational collapse at the shelf-edge rollover zone (SERZ) (e.g. Jackson & Johnson, 2009; Kneller *et al*., 2016) (Fig. 1A). Seismic-reflection datasets commonly image these features (e.g. Fulthorpe *et al*., 2000; Sylvester *et al*., 2012; Prélat *et al*., 2015) but generally lack bed-scale to bedset-scale information on the process response to changing margin physiography during phases of degradation and aggradation (Neal & Abreu, 2009). Outcrop studies allow an accurate analysis of sedimentary processes in channelized shelf-edge rollover deposits (e.g. Mellere *et al*., 2002; Petter & Steel, 2006),

but they are commonly based on rwo-dimensional stratigraphic cross-sections parallel to depositional dip and generally lack along-margin context.

This paper documents the depositional architecture of exhumed Permian basin-margin clinothems of the Karoo Basin, South Africa, which are cut by a 1.5 km wide and 100 m deep erosion surface. The outcrops expose seismic-reflection-scale clinoform geometries with three-dimensional constraints and a sub-seismic-reflection-scale process record with both depositional dip and strike control. The specific objectives are: (i) to present the detailed (centimetre to metre-scale) stratigraphy and sedimentology of the clinothem succession; (ii) to discuss the origin, infill and implications of a large-scale erosion surface in the transition from upper slope to shelf edge; and (iii) to interpret the basin margin evolution and controls on the timing of sediment delivery to the basin.

GEOLOGICAL SETTING

The study area is located in the Tanqua depocentre, in the south-western Karoo Basin, South Africa (Fig. 2A). The Karoo Basin was traditionally interpreted as a retroarc foreland basin, developed north of the Cape Fold Belt (CFB) from the early Permian (Johnson, 1991; Cole, 1992; Visser, 1993; Veevers *et al.,* 1994; Catuneanu *et al.,* 1998). However, more recent models relate subsidence during the Permian to long-wavelength dynamic topography driven by the subducting palaeo-Pacific plate (Tankard *et al.,* 2009) with no emergent Cape Fold Belt at the time of deposition of the deep-water to shelf succession. Petrographic work suggests that most of the Permian sediments were derived from the Patagonian massif (Johnson, 1991; Van Lente, 2004; King *et al.,* 2009) prior to opening of the southern Atlantic Ocean. The narrow grain-size range of Karoo Basin sediments (generally fine siltstone to fine sandstone) is consistent with a mature source and relatively long sediment transport distance.

The sedimentary fill of the Karoo Basin comprises the Karoo Supergroup, an overall shallowing-upward succession (Smith, 1990) (Fig. 2D). Deposition initiated with Late Carboniferous glacial sediments of the Dwyka Group and the subsequent glacial retreat (Visser, 1997; Bangert *et al.,* 1999;

Isbell *et al.,* 2008) that is marked by the Permian Prince Albert, Whitehill and Collingham formations (Visser, 1994; Scheffler *et al.,* 2006; Johnson *et al.,* 2006). In the Tanqua depocentre, these deposits are overlain by *ca* 800 m of mudstones of the Tierberg Formation (Fig. 2D; King *et al.,* 2009). The overlying Skoorsteenberg Formation comprises sandstone-rich basin-floor fans 1 to 4 (Bouma & Wickens, 1991; Wickens, 1994; Johnson *et al.,* 2001; Hodgson *et al.,* 2006) and a channelized slope wedge (Unit 5, Wild *et al.,* 2005; Hodgson *et al.,* 2006). This study focuses on the overlying upper slope to shelf sediments of the Waterford Formation (Wickens, 1994; Wild *et al.,* 2009; Dixon *et al.,* 2012; Gomis-Cartesio *et al.,* 2017; Laugier and Plink-Björklund, 2016; Poyatos-More *et al.,* 2016; Fig. 2D), the lower part of which was originally assigned as the Kookfontein Formation (Wickens, 1994). The studied succession also includes the transition to terrestrial conditions recorded by the fluvial Abrahamskraal Formation of the Beaufort Group (Smith, 1990; Johnson *et al.,* 2006; Gulliford *et al.,* 2014; Wilson *et al.,* 2014) (Fig. 2D).

DATASET AND METHODS

The Waterford Formation is exposed over *ca* 1600 km^2 in the north-eastern part of the Tanqua depocentre (Fig. 2B). This study is focused on the Geelhoek locality (14 km^2, Figs 2C and 3A). The exposure is 500 to 750 m high, with a *ca* 5 km long SSW–NNE and *ca* 4 km-long WSW–ENE arcuate shape that allows good three-dimensional reconstructions (Fig. 2C).

Eight regional (1:50 scale) sedimentary logs (up to 500 m thick with 2340 m of cumulative logged section) were measured and correlated to build the stratigraphic framework (Figs 3A, 3B and 4A). High-resolution correlation using 31 detailed logs and field sketches record the nature of contacts and bounding surfaces. Stratigraphic surfaces were walked between logs and supplemented by interpretation of satellite, oblique helicopter and unmanned aerial vehicle photographs and facies mapping (Fig. 3C). Four key surfaces were mapped with time-averaged GPS waypoint measurements. Fitting a surface to the waypoints using the kriging function of ArcGIS obtained 3D planes of each surface, which enabled the calculation of maximum dip orientation and magnitude

(Fig. 3B). Palaeocurrent distribution was constrained through 794 measurements of planar and trough cross-bedding foresets, ripple-cross lamination, primary current lineation, basal tool marks and channel-margin orientations (Fig. 4B).

LITHOFACIES AND FACIES ASSOCIATIONS

Table 1 summarizes a process-based lithofacies scheme, which includes textures and sedimentary structures. Facies Associations 1 to 4 (summarized in Table 2) are used to characterise architectural elements and their interpreted environment of deposition and are based on Gomis-Cartesio *et al*. (2017). New facies associations (A, B and C) are introduced to complement those described in Table 2.

Facies Association A – Structureless and erosive sandstone-dominated deposits

Description

Lenticular packages of thick-bedded (1 to 6 m thick) medium-grained, fine-grained and very fine-grained sandstones with highly erosional bases. Bed thickness can vary from a few centimetres to several metres either because they are partly eroded or because they thin and/or onlap onto underlying surfaces. Bed bases and amalgamation surfaces have a high concentration (up to 1 m thick) of mudstone clasts, with subsidiary clasts of sandstone, carbonate or siltstone (Fig. 5). Sandstones are poorly sorted with common mudstone chips and plant fragments throughout. Typically, beds are normally graded, and pass upward from structureless to parallel-laminated or cross-bedded to climbing-ripple-laminated (Fig. 5). Undulate and high-angle cross-bedding are also observed, as well as loading structures. Bed sets normally display a fining-upward and thinning-upward motif. Locally, beds show soft sediment deformation horizons.

Interpretation

The main characteristic of this facies association is the relatively high proportion of erosive features (up to 6 m deep), cut and fill geometries and amalgamation of sandstone bodies. Structureless, erosive and amalgamated sandstones with weak normal grading suggest rapid deposition from sand-rich high-density turbidity currents (Lowe, 1982; Mutti *et al.,* 2003; Talling *et al.*, 2012), together with processes such as seabed erosion and entrainment, and pervasive dewatering (Hodgson *et al.*, 2006; Prélat *et al.*, 2009; Hofstra *et al.*, 2015). Cross-bedding in deep-water sandstones has been reported in other parts of the basin and associated with continued reworking of the substrate by efficient, long-lived turbidity currents (Grecula *et al.,* 2003; Brunt *et al.,* 2013). Basal mudstone clast horizons associated with bedding surfaces are interpreted as residual lag deposits of material eroded and left behind by largely bypassing flows (Stevenson *et al.,* 2015); their presence on down dip inclined surfaces has been associated with transient bedforms, such as dunes within channel-fill complexes (Brunt *et al.,* 2013).

Facies Association B – Traction-dominated sandstone/siltstone deposits

Description

Laterally discontinuous packages of thick to thin-bedded siltstones to fine-grained sandstones (3 m to a few centimetres thick) confined by concave-up, tens of metres wide erosion surfaces that truncate underlying bedding (Fig. 6). Multiple internal amalgamation surfaces are common within the thicker units (Fig. 6). Commonly, basal surfaces are overlain by mudstone clast horizons. Sandstones are clean, normally graded and dominated by climbing-ripple and current-ripple cross-lamination (Fig. 6). In a few cases, structureless or parallel-laminated subdivisions can be observed at the bed bases.

Interpretation

The high proportion of traction structures and the confinement of beds or bed sets within narrow and concave-up erosive surfaces are consistent with rapid deposition from low-density turbidity currents within conduits or scours (Wild *et al.,* 2005; 2009). Climbing-ripple lamination in normally graded sandstones has been observed in deposits of different deep-water depositional environments in the Karoo Basin (Grecula *et al.,* 2003; Brunt *et al.,* 2013; Morris *et al.,* 2014; Spychala *et al.,* 2015) and is typically associated with high sedimentation rates (Jobe *et al.,* 2012).

Facies Association C – Inverse to normal-graded, siltstone-dominated deposits

Description

Laterally-discontinuous packages of interbedded 1 m to 1 cm thick micaceous siltstone and very fine-grained sandstone confined by concave-up erosion surfaces (Fig. 7). Gradational contacts dominate (Fig. 7), beds are usually sub-horizontal and woody fragments are common. There is a dominance of gradual and subtle grain-size variations from siltstone to very fine-grained sandstone in inverse to normally-graded grain-size trends (Fig. 7). These siltstone-prone composite beds (<1 m thick) are dominated by structureless or parallel-laminated subdivisions. Locally, unidirectional, starved or inversely-graded climbing ripples are observed in the middle portion of the beds, where the grain size is coarser.

Interpretation

The high proportion of diffuse, inverse to normal-graded composite beds, contained within subtle erosion surfaces are interpreted to represent traction plus fallout processes in waxing to waning dilute gravity flows in relatively unconfined settings. The grain-size grading patterns and presence of organic fragments and mica suggest a hyperpycnal origin and may indicate a direct or partial fluvial connection (e.g. Mulder *et al.,* 2003; Plink-Björklund & Steel, 2004; Bhattacharya & MacEachern,

2009; Zavala *et al.,* 2011; Poyatos-Moré *et al.,* 2016). The vertical transition from Facies Association B to C may indicate a genetic relationship but in a more distal or off-axis position.

SHELF-MARGIN ARCHITECTURE

The *ca* 600 m-thick shallowing-upward succession has been subdivided into 10 coarsening-upward units interpreted as parasequences (*sensu* Van Wagoner *et al.,* 1990; Figs. 3B and 4A). Parasequence boundary flooding surfaces are readily recognizable and mappable in the lower part of the succession, where they involve offshore deposits. The upper units are thinner and more amalgamated, making flooding surfaces more difficult to recognize.

Basal aggradational to progradational phase (Parasequences P1 to P3)

The lower 175 m of the succession comprises Parasequence 1 (P1, 70 m thick), Parasequence 2 (P2, 55 m thick) and Parasequence 3 (P3, 50 m thick) (Figs 3B and 4A), each of which is characterised by lower mudstone-rich offshore deposits (FA-1), passing upward into distal prodelta heterolithic deposits (FA-2i) and, in the case of P2 and P3, to proximal prodelta deposits (FA-2ii). At the base of P1, a 1 to 2 m thick normally graded medium to fine-grained sandstone is found (Fig. 4A). At the base of the sandstone, a mudstone clast conglomerate containing large wood pieces (up to 5 cm long) grades up from fine, dirty (argillaceous) structureless sandstone to climbing-rippled sandstone (similar to Facies Association A). Ripple cross-lamination indicates north-east-directed palaeoflow, while the orientation of wood fragments and sole marks show north-east/south-west and north-west/south-east directions (Fig. 4B). Bioturbation is generally low [bioturbation index (BI) 1 to 2]. Cone in cone nodules or layers are common within the mudstone succession of P1.

Four smaller-scale coarsening-up bedsets can be recognized in P2 and two in P3, but only the flooding surfaces marking the top of both parasequences can be mapped regionally (Figs 3B and 4A). Current-ripple and climbing-ripple lamination is common in normally-graded and/or inversely-graded sandstones with palaeocurrents towards the north-west, north and north-east. Symmetrical-

rippled bed tops show a north-east/south-west direction of reworking (Fig. 4B). Bioturbation is moderate to high (BI 3 to 4).

Parasequence 1 is correlated with deposits interpreted as slope turbidites further south by Gomis-Cartesio *et al*. (2017) (Fig. 2B). Parasequence2 and 3 deposits are dominated by traction and fallout processes from dilute turbidity currents, developed distally or laterally from denser hyperpycnal flows, the deposits of which are observed towards the upper parts of the units. There is no exposure of P1 to P3 in the central part of the outcrop due to the structural dip towards the north/north-east. However, the thinning of the sandstone beds and the progressive transition from sandstone-rich to siltstone-rich heterolithic deposits suggest a change from proximal (south/south-west) to distal (north/north-east) settings along the 3 km outcrop face (Fig. 3B).

Maximum regression phase (Parasequences P4 and P5)

Parasequence 4 (P4)

Parasequence 4 is approximately 75 m thick (Figs 3B and 4A) and includes offshore to prodelta deposits (FA-1 and FA-2) and the first appearance of mouth-bar and channelized deposits (FA-3). A <25 m-thick package of tabular and thin to thick-bedded (0.2 to 3.0 m thick) sandstones forms the top of P4 (Figs 3B and 4A). Siltstone and sandstone beds are dominantly climbing and current ripple laminated, with rare symmetrical-rippled bed tops, interpreted as indicating minor wave or storm reworking. Towards the upper part of P4, low-angle cross-laminated and structureless sandstones form packages up to 3 m thick. Amalgamation surfaces with mudstone clasts, loaded bases or deformed beds are also observed. A concave-up, 20 m wide and 2 to 5 m deep erosion surface cuts into the upper part of P4. Unidirectional palaeocurrents are dominantly towards the north, and north-east/south-west bidirectional indicators are similar to the underlying parasequences (Fig. 4B). Bioturbation is low to moderate (BI 1 to 3).

The upper part of P4 shows a progressive north/north-east down dip change (over hundreds of metres) from tabular, thick-bedded (FA-3) to intensely deformed sandstones (FA-4). Loading increases at the bed and bedset scale until beds are completely disaggregated and internal structures can be no longer recognized. Deformed beds are dominant in the upper part of P4 on the northern side of the correlation panel (GHn and GHm) and in GH1 (Figs 3B and 6). Parasequence 4 is interpreted to contain undeformed mouth bar and distributary channel deposits in the south-west, which get progressively deformed down-dip to the north-east.

Parasequence 5 (P5)

Parasequence 5 is relatively thin (<15 m thick) and its coarsening and thickening-upward trend starts with sandstone-dominated deposits (FA-2ii and FA3, Table 2; Figs 3B and 4A). Characteristically, P5 comprises coarser-grained (fine to medium-grained), poorly-sorted sandstones with high mudstone content, mudstone rip-up clasts and a higher bioturbation index (BI 3 to 5). In the bedded and interbedded packages, beds are either structureless or display climbing or unidirectional ripples and parallel lamination. Symmetrical-rippled bed tops are common, and low-angle cross-bedding is also observed in the thicker beds. Mudstone drapes are abundant. Unidirectional palaeocurrents show a wide range of dispersal directions, from south-west to north-east, although symmetrical-ripple orientation remains consistent (north-east/south-west, Fig. 4C). In the south (GH6), the top of P5 shows metre-scale mudstone-prone coarsening and thickening-upward packages from laminated fine to coarse siltstone or very fine sandstone or to mixed sandstone–siltstone debrites (FA-4), with abundant plant fragments and bioturbated tops; their stacking pattern and facies have been associated with delta plain deposits (Wickens, 1994; Rubidge *et al.,* 2000; Wilson *et al.,* 2014). The coarser and poorly sorted character of P5 sandstones is consistent with a more proximal depositional environment relative to P4. The large amount of rip-up clasts suggests high energy flows, while the high bioturbation index indicates times of relative quiescence and colonization by organisms, suggesting fluctuating environmental conditions. Parasequence 5 is only present in the

southern exposures of the Geelhoek locality, because it is removed by a major erosion surface towards the north that also truncates P4 and part of P3.

Degradation phase: the Geelhoek erosion surface and infill

Geometry

A 75 to 100 m deep and concave-up surface truncates the whole of P5, P4 and part of P3 towards the northern, more distal exposures (Figs 3, 8 and 9). In the south, detailed mapping and field description reveals that P5 is cut progressively via multiple erosion surfaces that coalesce between the GH6 and GH1 localities (Fig. 9A and B). These surfaces merge to form a composite surface that incises deeper into P4 from GH1 to GH5, where only the basal offshore mudstones of P4 are preserved (Figs 3, 8 and 9). Further north (GH4 to GH2) the top of P3 is also truncated (Figs 3 and 8). At the northern margin, although the lack of a clear lithological contrast across the surface makes it more difficult to follow, truncation of P5 and P4 seems to be more abrupt (Figs 3, 8 and 9C). The basal composite surface is observable at the bottom of log GH2 and progressively steepens towards GH1 and GHm, where it loses its angular geometry and becomes paraconformable with the underlying stratigraphy. Therefore, the basal surface is composite and asymmetrical, with a steeper (22°) northern margin and gentler (6°) southern margin (Figs 3 and 6).

Evidence for instability and erosion associated with the composite erosion surface are found in the GH1 section (Fig. 9B). The upper part of P4 is heavily deformed and the top of P5 shows large-scale erosion features. The transition from P5 to P6 is characterized by the presence of a large (10 m high and 20 m wide) block of soft-sediment deformed material that is detached or remobilized from its original position, and laterally eroded or faulted (Figs 3 and 8). Inclined interbedded sandstones and siltstones display a fan-like geometry and progressively shallower dips upward, suggesting either rotated blocks or growth strata (Figs 3 and 8) overlying this block.

Sedimentary fill

The nature of the sedimentary fill of the Geelhoek erosion surface and its stacking pattern is significantly different from the units below and above and comprises a fining-upward and thinning-upward succession (Figs 3A, 8 and 10). The basal 10 m is dominated by Facies Association A (Fig. 5). The overlying 40 m-thick middle section is dominated by Facies Associations B and C (Figs 6 and 7). The upper 50 m of fill shows a change to a coarsening-upward and thickening-upward succession associated with the distal expression of the next prograding parasequence P6 (see below, Figs 8 and 10).

The erosion surface is easier to map and recognize where there are overlying thick-bedded sandstones of Facies Association A. In the area between GH2 and GH5 (Fig. 8), basal sandstones show a highly erosive and sharp contact with the underlying siltstone-prone stratigraphy of P4 or P3 (Fig. 8). Here, sandstones of Facies Association A are the thickest (<5 m thick) and overlain by Facies Associations B and then C. Further up dip towards GH1, where the composite erosion surface cuts shallower facies of P4 (Fig. 8), sandstones of Facies Association A progressively onlap the major surface (Fig. 9A). Where sandstones are absent only mudstone-clast conglomerates (up to 0.7 m thick) are found overlying multiple erosion surfaces. Sandier and thicker-bedded Facies Associations B and C overlie the mudstone-clast conglomerates.

At the northern margin of the erosive surface (GHm), sandstones of Facies Association A pinch out more abruptly (Fig. 8), and where shallower deposits of P4 are eroded only Facies Association C is present. This may suggest that several of the erosional and depositional episodes that characterize the composite infill of the southern margin are not preserved on the steeper, northern margin (22°). In the deepest part of the cut (Fig. 10), each thick-bedded sandstone of Facies Association A erodes into an older one at an angle, with amalgamation surfaces younging towards the north and north-east. Up to 10 m of Facies Association A accumulated by this cut and fill process, forming a 'shingled' architecture (Figs 8 and 10), which suggests a significant phase of sediment bypass and erosion at the base of the cut (Stevenson *et al.,* 2015). Locally, the lowermost deposits of Facies Association B

erode into Facies Association A. Erosion surfaces preserved in traction-dominated Facies Association B show no preferential orientation and both sides of these subsidiary cuts are well-preserved in most cases (Fig. 7), suggesting that sediment bypass processes continued but less efficient. Facies Association C is found either overlying Facies Association B in the older fill components or overlying wider and younger erosive surfaces (Fig. 10). Beds in Facies Association C are progressively more bioturbated as they fine and thin upward.

The oldest deposits of P6 form the final infill of the erosive feature between GHm and GH1; their base comprises interbedded mudstone and siltstone packages that have a high bioturbation index (BI 4 to 5; the highest observed). Overlying these deposits, the coarsening-upward character is consistent with progradation of the upper part of P6 and can be seen along the entire outcrop, healing the remaining erosional topography and showing a relatively abrupt proximal to distal transition from south (GH6) to north (GH5).

Overall, the dip of beds and bedsets filling the Geelhoek incision decreases upwards, with basal bedsets dipping at nearly 30˚, decreasing to 2 to 3˚ towards the top (Fig. 10). This progressive dip reduction is linked to the upward decreasing frequency of erosive cuts and gullies and dip-shallowing of P6 foresets.

Upper aggradational to progradational phase (P6 to P10)

Parasequence 6 (P6)

Parasequence 6 is the first unit that can be correlated across the entire outcrop and thickens from 25 m in the southern outcrops (GH6) to more than 50 m over 1 km down dip to the north (GH5; Figs 3B and 8). In the south (GH6; Figs 3B and 8), P6 shows a vertical transition from FA-2i to FA-3ii (Table 2). The interbedded packages display a distinctive rhythmic pattern and cyclic arrangement (black and white colour alternation and a constant bed thickness for sandstone and siltstone beds). Sandstones and coarse siltstones are either structureless or show current or climbing ripples. Symmetrical-rippled bed tops are common. Towards the top, a complex alternation of interbedded

(FA-2) and *in situ* deformed packages (FA-4) dominates, although low-angle laminated thick-bedded sandstones are recognized. Deformed packages tend to amalgamate laterally and show lenticular shapes or fill concave-up surfaces, where flame and load structures are larger towards the thicker, axial parts. They are interpreted to be the result of loading and dewatering of thick-bedded sandstones. Further north, in the GH1 locality (Figs 3B and 8), deformation reaches its maximum expression with remobilized boulders and metre-scale flame structures. This intensely deformed top becomes less deformed along the first 100 m of exposure to the north (laterally, internal structures on beds are preserved).

In the northernmost exposures (GH5), P6 is thicker and preserves distal deposits passing from siltstone to sandstone-rich interbedded FA-1 to FA-2, in contrast to the dominance of FA-3 and FA-4 in the south (Fig. 4C). At the base, sedimentary structures are rare, and only starved ripples can be seen in the sandier laminae within dirty, organic rich, diffusely laminated and bioturbated (BI 3 to 4) siltstone packages. Rare lenticular, soft-sediment deformed or loaded beds and beds with symmetrical rippled tops are present towards the top of P6.

In this case, unidirectional palaeocurrents are dominantly to the north, but bi-directionality from symmetrical ripples and sole marks follows the dominant north-east/south-west trend (Fig. 4B). Distribution of facies suggests that during P6, wave-reworked and deformed delta lobes pass down dip into prodelta or shoreface-offshore transition deposits to the north (Fig. 4C). The distance over which these changes occur is only hundreds of metres, which contrasts with the 10 km scale of lateral change for those parasequences not affected by any major underlying incision. These changes in facies and thickness down dip are therefore significantly more abrupt in P6 than in other parasequences.

Parasequences 7 and 8 (P7 and P8)

Parasequences 7 and 8 are 20 m and 50 m thick in the south, respectively (Figs 3B and 4A), and thicken and show more distal facies towards the north (Fig. 4C); they contain bedsets with thin debrite layers at the base and wave-reworked or highly bioturbated tops. Detached pseudo-nodule deformation (Owen, 2003; Wild *et al.,* 2009; Oliveira *et al.,* 2011) is also common. Typically, these deformed beds are overlain by coarsening-upward and thickening-upward, well-defined interbedded packages of inversely to normally graded beds (FA-2) and thin- bedded and thick-bedded sandstones with parallel lamination or cross-stratification (FA-3). Commonly, mudstone clasts drape bedding and amalgamation surfaces. Overall, the degree of wave reworking, expressed as symmetrical ripple bed tops and hummocky cross-stratification in the interbedded packages (FA-2) and low-angle cross-bedding, hummocky or swaley cross-stratification within thin and thick-bedded sandstones (FA-3) is variable. However, unidirectional palaeocurrents and dirty (argillaceous) and organic-rich levels are not consistent with shoreface deposits, and therefore these parasequences are interpreted as mostly wave-dominated or wave-reworked deltaic deposits (e.g. Hampson, 2000; Bhattacharya & Giosan, 2003; Hampson & Howell, 2005). Unidirectional palaeocurrents from current ripples are dispersed (Fig. 4B), but north-east/south-west bi-directionality remains constant.

Parasequences 9 and 10 (P9 and P10)

Parasequences 9 and 10 are less variable in terms of thickness and lateral facies changes (Figs 3B and 4A); they still show coarsening and thickening-upward profiles but a relatively lower proportion of FA-2 and FA-3i (Fig. 4C). The number of symmetrical-rippled bed tops is generally less. Thick-bedded sandstones (FA-3) dominate, although abrupt alternations of organic matter-rich debrites and soft-sediment deformed beds (with detached pseudo-nodules) are found within fining-upward trends. Hummocky, swaley and unidirectional asymptotic cross-bedding associated with dune-scale unidirectional bedforms are the most common structures within thick-bedded sandstones (FA-3). In

P9, they normally amalgamate to form up to 10 m thick packages interpreted as shoreface or wave reworked delta top deposits and minor channel fills.

In P10, blocky mudstone-rich packages are more common between thick-bedded sandstones, forming coarsening-upward and thickening-upward packages. Sandstone bedsets are amalgamated and generally fine and thin upward. Low-angle to high-angle cross-bedding and parallel lamination are the most common sedimentary structures. Commonly, mudstone-clast lags mantle bedding and amalgamation surfaces. These deposits are interpreted as distributary channel-fills in a lower delta-plain setting. Above P10, coarsening-upward and thickening-upward trends are not recognized and generally thick-bedded sandstone channel-fills are overlain by fine-grained green mudstones and siltstones with a distinctive blocky texture. These deposits have been interpreted in this and other areas as fluvial channel-fills in a delta plain setting (Wickens, 1994; Rubidge *et al.,* 2000; Wilson *et al.,* 2014). Unidirectional palaeocurrent values from current ripples in P9 and P10 are highly dispersed (Fig. 4B) but bidirectionality from symmetrical bed tops shows a slight variation towards the NNE–SSW, possibly associated with higher ripple interference in shallower waters.

Shelf-margin setting

Regional mapping reveals that the Geelhoek succession is laterally equivalent to the Paardeberg ridge outcrop, 6 km to the south-east (Gomis-Cartesio *et al*., 2017) and exposes the equivalent stratigraphy. The shallowing upward succession is similarly defined by a lower mudstone-prone (P1) and a prodelta-dominated section (P2 and P3) deposited in an upper slope setting. The intermediate mixed-influence and deformed mouth-bar deposits of P4 to P6 are also interpreted as being deposited at the shelf-to-slope transition. The main difference between the two localities is that in Geelhoek, deposits of P5, P4 and P3 are truncated by the large-scale erosional surface. This influenced the character of the uppermost parasequences (P7 to P10), which are generally thinner, coarser-grained and shallower-water deposits that show strong wave reworking and bioturbation, all consistent with a much shallower shelf to delta-plain setting.

Correlation within Geelhoek shows that P6 to P10 are thicker towards the north, with more distal facies (Figs 3B and 8). This evidence, coupled with the dominant north/north-east palaeocurrents (Fig. 4B), supports a depositional dip direction from south-west to north-east. Maximum compacted slope angles obtained for the mapped top surfaces corrected for tectonic dip are 1.5° for the top of P6, 1.0° for the top of P9 and 0.7° for the top of P10.

DISCUSSION

Stratigraphic evidence for instability, erosion and infill processes at the shelf edge

The formation of the Geelhoek composite erosion surface and subsequent infill is interpreted to be a product of shelf-edge and upper-slope degradation and subsequent readjustment and healing. The box-like shape of the main erosion feature, with relatively steep walls (22° to 6°) and a flat base (Fig. 8), the large blocks of substrate with growth strata at the southern margin (GH1, Fig. 9A and B), and the observation that this scale of feature is not recognized elsewhere in the study area may suggest a localized initial mass-wasting event, resulting in a large (<100 m deep and <2 km wide) slide scar with steep lateral margins. This size is comparable to several submarine landslides documented along the US Atlantic continental slope (Chaytor *et al*., 2009). Growth faulting, sliding or slumping are common mechanisms of shelf-edge degradation (Edwards, 1981; Winker & Edwards, 1983; Suter & Berryhill, 1985; Coleman & Prior, 1988; Sydow & Roberts, 1994; Hampton *et al.,* 1996; Porębski & Steel, 2003; Jackson & Johnson, 2009). However, no destabilization indicators such as large (tens of metres thick) remobilized deposits at the base of the infill or extensional faults at the margins have been found to support the hypothesis of a single, gravitational collapse. Outcrop limitations do not permit investigation of potential gravitational collapse deposits further down dip. Deposits filling the erosional feature are significantly different to those found outside it (Fig. 8), which suggests that local sliding or slumping were not the only processes involved in the infill of the incision.

The composite nature of the basal erosion surface indicates the existence of more than a single erosion event and suggests that the cut acted as a long-lived conduit that bypassed sediment into the deeper basin (e.g. Winn & Dott, 1977; Mutti & Normark, 1987; Pickering *et al.*, 2001; Hodgson *et al.,* 2011; Macauley & Hubbard, 2013; Stevenson *et al.,* 2015). Multiple erosion surfaces recognized towards the margins (GH1) and the vertical passage from Facies Association A to B and C in the fill (Fig. 10) indicates a transition from sediment bypass-dominated processes (Facies Association A) to deposition-dominated processes (Facies Associations B and C). This fining-upward and thinning-upward stacking pattern has been related to the equilibrium dynamics of submarine conduits, and supports the interpretation of a submarine canyon-fill (e.g. Mutti, 1985; Mutti & Normark, 1987; Pratson *et al.,* 1994; Pickering *et al.,* 1995; Fulthorpe *et al.,* 1999; 2000; Plink-Björklund & Steel, 2002; Kneller, 2003; Posamentier & Kolla, 2003; Petter & Steel, 2006; Walsh *et al.*, 2007; Hodgson *et al.,* 2011; McHargue *et al.,* 2011; Figueiredo *et al.,* 2013; Janocko *et al.,* 2013; Fildani *et al.,* 2013: Hubbard *et al.,* 2014; Prélat *et al.,* 2015). During formation of a submarine conduit there is a steep axial gradient, and confinement and sediment bypass dominates in the upper slope. Deposition occurs further down-dip, because most of the flows are able to bypass the area while eroding and shaping the walls of the canyon (e.g. Winn & Dott, 1977; Mutti & Normark, 1987; Hubbard *et al.,* 2014; Stevenson *et al.,* 2015). During the evolution of the canyon, deposition down-slope and erosion up-slope leads to a progressive decrease in the axial gradient, such that flows become less efficient and more depositional (e.g. Hodgson *et al.,* 2016). Therefore, the vertical evolution of the fill could be attributed to an autocyclic response to the local creation and filling of accommodation around the shelf to slope transition, in order to restore the equilibrium or 'graded' profile of the clinothem (Ross *et al.,* 1994; 1995; Prather *et al.,* 2003). In the Geelhoek locality, this is shown by the fining-upward and thinning-upward motif and progressive onlap of turbidites against the underlying and eroded deposits of P3 and P4 (Fig. 9).

The Geelhoek feature is not a slope-confined blind canyon or slope-sourced canyon because the head does not terminate below the shelf-edge rollover (Shepard, 1972; 1981; Greene *et al.,* 1991;

Jobe *et al.,* 2011; Brothers *et al.,* 2013). The erosion surface truncates proximal deltaic deposits of P4 and P5 (Fig. 8), and is therefore a shelf-incised canyon, a common situation observed in modern systems (e.g. Walsh *et al.*, 2007; Walsh & Nittrouer, 2009; Dalla Valle & Gamberi, 2011) but rarely identified at outcrop (e.g. Nijman, 1998; Payros *et al.*, 2009). The presence of pedogenic carbonate clasts within Facies Association A (Fig. 5), relatively large (up to 40 cm radius) well-preserved fragments of petrified wood in Facies Association B and the hyperpycnal character of beds in Facies Association C suggest a direct or partial fluvial connection existed at the head of the canyon (Figs 5, 6 and 7). This range of characteristics indicate a combined mechanism of formation, with an initial degradation phase through sliding or slumping, and subsequent modification by multiple gravity flows that first bypassed and then infilled a slope canyon.

Shelf margin architecture and sequence stratigraphy

The 600 m thick succession, from basin floor to continental deposits, records the complete vertical evolution of the basin margin (Figs 3 and 11). Parasequences 1 to 5 represent an aggradational to progradational parasequence set (*sensu* Neal & Abreu, 2009) (Fig. 11A, B and C), interpreted as part of a highstand systems tract. The maximum regression is recorded by the most proximal deltaic facies associations of P5. A subsequent degradation stage culminated with the generation of a large composite erosive surface in the Geelhoek locality (Fig. 11C and D). The canyon initiated as a consequence of the oversteepening of a sandy channelized shelf-edge rollover zone, associated with a lowering of relative sea level and sequence boundary formation. The absence of subaerial exposure features at the canyon margins suggests that the relative sea-level fall was insufficient to expose the shelf edge in the study area. The basal erosional surface can be physically followed outside the incision, where it records a complex and composite surface containing both the subaqueous interfluve expression of the sequence boundary, and the overlying maximum flooding surface. The observed facies and stacking pattern of the canyon-fill represent a retrogradational stage, expressed by the first 50 m thick fining-upward and thinning-upward profile from the base of

the cut to the middle part of the fill (Fig. 11E). This pattern is interpreted to record early lowstand bypass and partial time-transgressive fill of onlapping and aggrading gravity flow deposits. The overlying siltstone-dominated, highly bioturbated and sandstone-starved package is interpreted to record the maximum point of transgression (Fig. 8), above which P6 prograded into the remaining underfilled accommodation (Fig. 9F). The upward decrease in the dip of lower P6 beds (from 10° to 2°, Fig. 10) reflects their progressive downlap onto the bioturbated, condensed siltstone. Parasequences 6 to 10 show an aggradational to progradational stacking pattern that healed the underfilled erosional topography (Fig. 11G), thus re-establishing an 'in-phase' equilibrium profile of the margin (*sensu* Ross *et al.,* 1994), and is consistent with a second highstand systems tract (Figs 3 and 11). This progressive shallowing pattern is commonly observed in seismic-reflection examples of either slides or canyons, which are filled by steeper dipping strata until they show a complete healing (e.g. Walsh *et al.*, 2007; Ryan *et al.,* 2009; Sylvester *et al.,* 2012; Prather *et al.,* 2016; Gamberi *et al.,* 2017) (Figs 1 and 11).

Origin and migration of erosional features

The progradational trajectory from P1 to P4 and the regressive character of the upper P4 and P5 deposits, with proximal mouth bars and distributary channel-fills, suggest that deposition created an increasingly steep shelf margin, resulting in local 'out of grade' conditions (Dailly, 1983; Ross *et al.,* 1994) during deposition of P5 (Fig. 11). Abundant soft-sediment deformation is present in P4 and P5, coincident with the higher values in clinothem gradient (map P4, Fig. 3C). These observations support the interpretation of parasequence P5 prograding over a relatively steep sand-rich shelf-edge rollover zone developed in P4 in this area.

In the Paardeberg outcrop, 6 km across strike to the south-east (DR locality, Figs 2B and 12), proximal mouth bars and distributary channel-fills of the 'middle unit' described by Gomis-Cartesio *et al.* (2017) are correlated to P4 at Geelhoek (Fig. 12). Both sections therefore record sand-dominated deposition in a shelf-edge position during the same period. The presence of older, minor

gulley development in the upper slope (Gomis-Cartesio *et al.*, 2017), could probably represent the early expression of a degradation stage that progressively migrated from south-east to north-west (Figs 12 and 13) and culminated in the Geelhoek locality area with the generation of the shelf-incised canyon during P5 (Fig. 13). The migration of shelf-edge degradation can result from the autocyclic interaction between existing and buried gulleys and the lateral compensation of prograding deltaic lobes/mouth bars (e.g. Pratson *et al.*, 1994) (Fig. 13). The increase in scale of degradation northward may also indicate a potentially-predictable link between minor, predecessor conduits and much larger erosive features along strike and through time (Gee & Gawthorpe, 2007; Sylvester *et al.*, 2012) (Fig. 13).

However, the fact that the same stacking pattern, with two well-defined prograding and shallowing-upward successions (P1 to P5 and P6 to P10) is seen along the entire >70 km northern part of the Tanqua depocentre also supports an allocyclic control on the stratigraphic evolution of the basin margin. The abrupt progradation of paralic systems to the shelf edge (starting at P4 time), plus the combination of lateral variability in the dominant process regime and sediment distribution along-strike led to higher supply and local oversteepening in certain areas (Olariu & Steel, 2009; Olariu *et al.*, 2012; Sanchez *et al.*, 2012; Jones *et al.*, 2015). At Geelhoek, this contributed to the generation of a shelf-incised canyon system, which would have been enhanced during a relative sea-level fall.

Subsurface implications

This study provides a rare example of exhumed basin-margin clinothems with good three-dimensional constraints and sub-seismic-reflection-scale details. The scale and geometry of the Geelhoek canyon (1.5 km wide and 100 m deep) is comparable with examples identified in many seismic-reflection datasets (e.g. Sanchez *et al.*, 2012; Sylvester *et al.*, 2012; Brothers *et al.*, 2013). Figure 1 shows how healing of negative topography by progradation of steeper clinothems is a common feature recognized in seismic-reflection datasets, independent of the origin of the space created. Shelf-edge degradation through destabilization or erosion is a process generally resulting in

mass-transport deposits or formation of submarine valleys, canyons or channel complexes (e.g. Pickering *et al.,* 1995; Kneller, 2003; Mayall *et al.,* 2006; 2010; McHargue *et al.,* 2011; Sylvester *et al.,* 2011; Hodgson *et al.,* 2011; Figueiredo *et al.,* 2013; Hubbard *et al.,* 2014). The filling of these conduits is generally during transgression and backstepping or through progradation and healing, or a combination of both. The Geelhoek study shows the architecture and detail of this healing process and provides criteria to recognize it in the absence of large-scale geometrical data. The location and nature of shelf-incised canyon margins and the expression of equivalent surfaces in their proximal landward termination can be complex to assess. The interfluve areas may appear paracomformable and the details may be difficult to observe, except in few high-resolution seismic-reflection datasets (Sylvester *et al.,* 2012). Similar examples resembling the Geelhoek canyon-fill and the upper slope gullies at the Ouberg Pass–Paardeberg Ridge locality (Figs 12 and 13) could easily be attributed to the same regressive phase. However, correlation suggests that the Geelhoek canyon-fill is slightly younger and not necessarily connected to the smaller conduits in the south, which has important implications for the timing and prediction of sediment bypass to positions further basinward.

CONCLUSIONS

1   Ten shallowing-upward parasequences (P1 to P10) form a prograding set of exhumed basin margin clinothems in the Geelhoek locality. These clinothems comprise upper slope deposits (P1 to P3), mixed-influence mouth bars at the shelf edge (P4 to P6) and thinner and coarser shelf to delta-plain facies associations (P7 to P10). Parasequences P3 to P5 are truncated by a 100 m deep, 1.5 km wide concave-up erosion surface that is composite and asymmetrical. The fill includes basal mudstone-clast conglomerates mantling multiple surfaces and thick-bedded sandstones with highly erosive contacts and a 'shingled' architecture. These are overlain by thin-bedded hyperpycnal deposits that fill gulley scours. Prograding deposits of parasequence P6 downlap and fill the remaining accommodation. The steep margins of the incision could support an origin by local mass-

wasting, although composite erosion surfaces indicate more than a single sediment bypass period and suggest that the negative topography acted as a relatively long-lived shelf-incised canyon.

2 The aggradational-to-progradational stacking of parasequences P1 to P5 are consistent with a highstand systems tract. A maximum regression and degradation stage during P5 culminated with the development of a large erosive surface, associated with a lowering of relative sea level and sequence boundary formation, but without subaerial exposure of the shelf edge. The 50 m thick retrogradational fining-upward and thinning-upward deposits within the cut represent lowstand bypass and a partial time-transgressive fill. A highly bioturbated siltstone package records the maximum transgression within the canyon. The subaqueous interfluve is a composite surface, containing both the sequence boundary and the overlying maximum flooding surface. Parasequences P6 to P10 show an aggradational to progradational stacking pattern consistent with a second highstand systems tract that healed the topography, re-establishing an 'in-phase' equilibrium profile.

3 Regional correlation indicates that the Geelhoek canyon-fill lies across strike from a highly incised, sandstone-rich shelf-edge rollover zone 6 km to the south-east. This suggests a period of widespread oversteepening along the shelf margin, and south-east to north-west migration of conduit position in the shelf to slope transition. This migration resulted from the autocyclic interaction between existing and buried conduits and lateral compensation of prograding deltaic lobes. The increase in degradation northward indicates a predictable link between minor, predecessor upper slope conduits and much larger erosive features along strike and through time. However, the same stacking pattern along the entire northern part of the Tanqua depocentre supports an allocyclic control of the stratigraphic evolution of the basin margin.

4 This study provides a rare outcrop example of seismic-reflection-scale clinothem degradation and readjustment with documentation of sub-seismic-reflection detail, and suggests that the presence of large-scale sediment bypass features along strike can be represented by subtle breaks in the dominant stacking pattern or the appearance of multiple erosive surfaces in the

'interfluve' areas. Large-scale clinothem degradation can occur in overall strongly progradational systems and large volumes of sediment can be therefore expected in basinward positions without subaerial exposure of the shelf-edge.

REFERENCES

Adams, E.W. and Schlager, W. (2000) Basic Types of Submarine Slope Curvature. *Journal of Sedimentary Research*, **70,** 814-828.

Bangert, B., Stollhofen, H., Lorenz, V. and Armstrong, R. (1999) The geochronology and significance of ash-fall tuffs in the glaciogenic Carboniferous-Permian Dwyka Group of Namibia and South Africa. *Journal of African Earth Sciences*, **29,** 33-49.

Bhattacharya, J.P. and Giosan, L. (2003) Wave-influenced deltas: geomorphological implications for facies reconstruction. *Sedimentology*, **50**, 187–210.

Bhattacharya, J.P. and MacEachern, J.A. (2009) Hyperpycnal rivers and prodeltaic shelves in the Cretaceous seaway of North America. *Journal of Sedimentary Research*, **79**, 184–209.

Bouma, A.H. and Wickens, H.d.V. (1991) Permian passive margin submarine fan complex, Karoo Basin. South Africa: possible model to Gulf of Mexico. *Gulf Coast Association of Geological Societies Transactions*, **41,** 30-42.

Brothers, D.S., ten Brink, U.S., Andrews, B.D. and Chaytor, J.D. (2013) Geomorphic characterization of the U.S. Atlantic continental margin. *Marine Geology*, **338,** 46-63.

Brunt, R. L., Hodgson, D. M., Flint, S. S., Pringle, J. K., Di Celma, C., Prélat, A. and Grecula, M. (2013) Confined to unconfined: anatomy of a base of slope succession, Karoo Basin, South Africa. *Marine and Petroleum Geology*, **41**, 206-221.

Carvajal, C. and Steel, R. (2009) Shelf-edge architecture and bypass of sand to deep water: influence of shelf-edge processes, sea level, and sediment supply. *Journal of Sedimentary Research*, **79,** 652-672.

Carvajal, C., Steel, R. and Petter, A. (2009) Sediment supply: The main driver of shelf-margin growth. *Earth-Science Reviews*, **96,** 221-248.

Catuneanu, O., Hancox, P.J. and Rubidge, B.S. (1998) Reciprocal flexural behaviour and contrasting stratigraphies: a new basin development model for the Karoo retroarc foreland system, South Africa. *Basin Research*, **10,** 417-439.

Cole, D.I. (1992) Evolution and development of the Karoo Basin. In: *Inversion Tectonics of the Cape Fold Belt, Karoo and Cretaceous Basins of Southern Africa* (Eds M.J. de Wit and I.G.D. Ransome), pp. 87-99, A.A. Balkema, Rotterdam.

Coleman, J.M. and Prior, D.B. (1988) Mass wasting on continental margins. *Annual Review of Earth and Planetary Sciences,* **16,** 101-119.

Covault, J.A., Romans, B.W. and Graham, S.A. (2009) Outcrop expression of a continental-margin-scale shelf-edge delta from the Cretaceous Magallanes Basin, Chile. *Journal of Sedimentary Research*, **79,** 523-539.

Dailly, G.C. (1983) Slope readjustment during sedimentation of continental margins. In: *Studies in continental marine geology. American Association of Petroleum Geologists Memoir 34* (Eds J.S. Watkins and C.L. Drake), pp. 593-608.

Dalla Valle, G. and Gamberi, F. (2011) Slope channel formation, evolution and backfilling in a wide shelf, passive continental margin (Northeastern Sardinia slope, Central Tyrrhenian Sea). *Marine Geology*, **286,** 95-105.

Dixon, J.F., Steel, R.J. and Olariu, C. (2012a) River-dominated, shelf-edge deltas: delivery of sand across the shelf break in the absence of slope incision. *Sedimentology*, **59,** 1133-1157.

Dixon, J.F., Steel, R.J. and Olariu, C. (2012b) Shelf-edge delta regime as a predictor of deep-water deposition. *Journal of Sedimentary Research*, **82,** 681-687.

Edwards, M.B. (1981) Upper Wilcox Rosita delta system of South Texas; growth-faulted shelf-edge deltas. *AAPG Bulletin*, **65,** 54-73.

Figueiredo, J.J.P., Hodgson, D.M., Flint, S.S. and Kavanagh, J.P. (2013) Architecture of a channel complex formed and filled during long-term degradation and entrenchment on the upper submarine slope, Unit F, Fort Brown Fm., SW Karoo Basin, South Africa. *Marine and Petroleum Geology*, **41,** 104-116.

Fildani, A., Hubbard, S.M., Covault, J.A., Maier, K.L., Romans, B.W., Traer, M. and Rowland, J.C. (2013) Erosion at inception of deep-sea channels. *Marine and Petroleum Geology*, **41,** 48-61.

Flint, S. A., Hodgson, D. M., Sprague, A. R., Brunt, R. L., Van der Merwe, W. C., Figueiredo, J., Prélat, A., Box, D., Di Celma, C. and Kavanagh, J. P. (2011) Depositional architecture and

sequence stratigraphy of the Karoo basin floor to shelf edge succession, Laingsburg depocentre, South Africa. *Marine and Petroleum Geology*, **28**, 658-674.

Fulthorpe, C.S., Austin, J.A. and Mountain, G.S. (1999) Buried fluvial channels off New Jersey: Did sea-level lowstands expose the entire shelf during the Miocene?. *Geology*, **27,** 203-206.

Fulthorpe, C.S., Austin, J.A. and Mountain, G.S. (2000) Morphology and distribution of Miocene slope incisions off New Jersey: Are they diagnostic of sequence boundaries?. *Geological Society of America Bulletin*, **112,** 817-828.

Gamberi, F., Breda, A., and Mellere, D. (2017). Depositional canyon heads at the edge of narrow and tectonically steepened continental shelves: Comparing geomorphic elements, processes and facies in modern and outcrop examples. *Marine and Petroleum Geology,* **accepted**.

Gee, M.J.R. and Gawthorpe, R.L. (2007) Early evolution of submarine channels offshore Angola revealed by three-dimensional seismic data. *Geological Society, London, Special Publications*, **277,** 223-235.

Gomis-Cartesio, L.E., Poyatos-Moré, M., Flint, S.S., Hodgson, D.M., Brunt, R.L. & Wickens, H. DeV. 2017. Anatomy of a mixed-influence shelf edge delta, Karoo Basin, South Africa. In: *Sedimentology of Paralic Reservoirs: Recent Advances.* (Eds Hampson, G. J., Reynolds, A. D., Kostic, B. & Wells, M. R.), *Geological Society, London, Special Publications*, **444**, 393-418. First published online July 14, 2016.

Grecula, M., Flint, S.S., Wickens, H.D., Johnson, S.D. (2003) Upward-thickening patterns and lateral continuity of Permian sand-rich turbidite channel fills, Laingsburg Karoo, South Africa. *Sedimentology,* **50**, 831-853.

Greene, H.G., Clarke, S.H. and Kennedy, M.P.Y. (1991) Tectonic Evolution of Submarine Canyons along the California Continental Margin. In: *From Shoreline to Abyss. SEPM Special Publication, Vol. 46* (Ed R.H. Osborne), pp. 231-248.

Gulliford, A.R., Flint, S.S. and Hodgson, D.M. (2014) Testing Applicability of Models Of Distributive Fluvial Systems Or Trunk Rivers In Ephemeral Systems: Reconstructing 3-D Fluvial Architecture In the Beaufort Group, South Africa. *Journal of Sedimentary Research*, **84,** 1147-1169.

Hampson, G.J. (2000) Discontinuity surfaces, clinoforms, and facies architecture in a wave-dominated, shoreface-shelf parasequence. *Journal of Sedimentary Research*, **70**, 325–340.

Hampson, G.J. and Howell, J.A. (2005) Sedimentologic and geomorphic characterization of ancient wave-dominated deltaic shorelines; Upper Cretaceous Blackhawk Formation, Book Cliffs, Utah, U.S.A. In: *River Deltas – Concepts, Models, and Examples* (Eds L. Giosan, L. and J.P. Bhattacharhya). SEPM Special Publications, 83, 133–154.

Hampton, M.A., Lee, H.J. and Locat, J. (1996) Submarine landslides. *Reviews of Geophysics*, **34,** 33-59.

Harding, R. (2015) *Evolution of the giant southern North Sea shelf-prism : testing sequence stratigraphic concepts and the global sea level curve with full-three dimensional control. Unpublished Ph.D. thesis*, University of Manchester, United Kigndom, 296 pp.

Hedberg, H.D. (1970) Continental margins from viewpoint of the petroleum geologist. *AAPG Bulletin*, **54,** 3-43.

Helland-Hansen, W., and Hampson, G. J. (2009) Trajectory analysis: concepts and applications. *Basin Research*, **21**, 454-483.

Helland-Hansen, W., Steel, R.J. and Sømme, T.O. (2012) Shelf genesis revisited. *Journal of Sedimentary Research*, **82,** 133-148.

Hodgson, D.M., Flint, S.S., Hodgetts, D., Drinkwater, N.J., Johannessen, E.P. and Luthi, S.M. (2006) Stratigraphic evolution of fine-grained submarine fan systems, Tanqua Depocenter, Karoo Basin, South Africa. *Journal of Sedimentary Research*, **76,** 20-40.

Hodgson, D.M., Di Celma, C.N., Brunt, R.L. and Flint, S.S. (2011) Submarine slope degradation and aggradation and the stratigraphic evolution of channel-levee systems. *Geological Society of London, Journal*, **168,** 625-628.

Hodgson, D.M., Kane, I.A., Flint, S.S., Brunt, R.L. and Ortiz-Karpf, A. (2016) Time-Transgressive Confinement On the Slope and the Progradation of Basin-Floor Fans: Implications For the Sequence Stratigraphy of Deep-Water Deposits. *Journal of Sedimentary Research*, **86,** 73-86.

Hofstra, M., Hodgson, D.M., Peakall, J. and Flint, S.S. (2015) Giant-scour fills in ancient channel-lobe transition zones: formative processes and depositional architecture. *Sedimentary Geology*, **329**, 98-114.

Hubbard, S.M., Covault, J.A., Fildani, A. and Romans, B.W. (2014) Sediment transfer and deposition in slope channels: Deciphering the record of enigmatic deep-sea processes from outcrop. *Geological Society of America Bulletin*, **126,** 857-871.

Hubbard, S.M., Fildani, A., Romans, B.W., Covault, J.A. and McHargue, T.R. (2010) High-relief slope clinoform development: Insights from outcrop, Magallanes Basin, Chile. *Journal of Sedimentary Research*, **80,** 357-375.

Isbell, J.L., Cole, D.I. and Catuneanu, O. (2008) Carboniferous-Permian glaciation in the main Karoo Basin, South Africa: Stratigraphy, depositional controls, and glacial dynamics. *Geological Society of America Special Papers*, **441,** 71-82.

Jackson, C.A.L. and Johnson, H.D. (2009) Sustained turbidity currents and their interaction with debrite-related topography; Labuan Island, offshore NW Borneo, Malaysia. *Sedimentary Geology*, **219,** 77-96.

Janocko, M., Nemec, W., Henriksen, S. and Warchoł, M. (2013) The diversity of deep-water sinuous channel belts and slope valley-fill complexes. *Marine and Petroleum Geology*, **41,** 7-34.

Jobe, Z.R., Lowe, D.R. and Uchytil, S.J. (2011) Two fundamentally different types of submarine canyons along the continental margin of Equatorial Guinea. *Marine and Petroleum Geology*, **28,** 843-860.

Jobe, Z.R., Lowe, D.R., and Morris, W.R. (2012) Climbing-ripple successions in turbidite systems: depositional environments, sedimentation rates and accumulation times. *Sedimentology*, **59**, 867-898.

Johannessen, E.P. and Steel, R.J. (2005) Shelf-margin clinoforms and prediction of deepwater sands. *Basin Research*, **17,** 521-550.

Johnson, M.R. (1991) Sandstone petrography, provenance and plate tectonic setting in Gondwana context of the southeastern Cape-Karoo Basin. *South African Journal of Geology*, **94,** 137-154.

Johnson, M.R., van Vuuren, C.J., Visser, J.N.J., Cole, D.I., Wickens, H.d.V., Christie, A.D.M., Roberts, D.L. and Brandl, G. (2006) Sedimentary rocks of the Karoo Supergroup. In: *The geology of South Africa* (Eds M.R. Johnson, C.R. Anhaeusser and R.J. Thomas), Geological Society of South Africa and Council for Geoscience, Pretoria, pp. 461-499.

Johnson, S.D., Flint, S., Hinds, D. and De Ville Wickens, H. (2001) Anatomy, geometry and sequence stratigraphy of basin floor to slope turbidite systems, Tanqua Karoo, South Africa. *Sedimentology*, **48,** 987-1023.

Jones, G.E.D., Hodgson, D.M. and Flint, S.S. (2015) Lateral variability in clinoform trajectory, process regime, and sediment dispersal patterns beyond the shelf-edge rollover in exhumed basin margin-scale clinothems. *Basin Research*, **27,** 657-680.

Kertznus, V. and Kneller, B. (2009) Clinoform quantification for assessing the effects of external forcing on continental margin development. *Basin Research*, **21,** 738-758.

King, R., Hodgson, D., Flint, S., Potts, G. and Van Lente, B. (2009) Development of subaqueous fold belts as a control on the timing and distribution of deepwater sedimentation: an example from

the southwest Karoo Basin, South Africa. In: *External Controls on Deep-Water Depositional Systems. SEPM Special Publication, 92* (Eds B.C. Kneller, O.J. Martinsen and B. McCaffrey), pp. 261-278.

Kneller, B. (2003) The influence of flow parameters on turbidite slope channel architecture. *Marine and Petroleum Geology*, **20,** 901-910.

Kneller, B., Dykstra, M., Fairweather, L., and Milana, J. P. (2016) Mass-transport and slope accommodation: implications for turbidite sandstone reservoirs. *AAPG Bulletin*, **100**, 213-235.

Laugier, F.J. and Plink-Björklund, P. (2016) Defining the shelf edge and the three-dimensional shelf edge to slope facies variability in shelf-edge deltas. *Sedimentology*, **63,** 1280-1320.

Lowe, D.R. (1982) Sediment gravity flows: II. Depositional models with special reference to the deposits of high density turbidity currents. *Journal of Sedimentary Petrology*, **52**, 279–297.

Macauley, R.V., and Hubbard, S.M. (2013) Slope channel sedimentary processes and stratigraphic stacking, Cretaceous Tres Pasos Formation slope system, Chilean Patagonia: *Marine and Petroleum Geology*, **41**, 146–162.

Mayall, M., Jones, E. and Casey, M. (2006) Turbidite channel reservoirs—Key elements in facies prediction and effective development. *Marine and Petroleum Geology*, **23,** 821-841.

Mayall, M., Lonergan, L., Bowman, A., James, S., Mills, K., Primmer, T., Pope, D., Rogers, L. and Skeene, R. (2010) The response of turbidite slope channels to growth-induced seabed topography. *AAPG Bulletin*, **94,** 1011-1030.

McHargue, T., Pyrcz, M.J., Sullivan, M.D., Clark, J.D., Fildani, A., Romans, B.W., Covault, J.A., Levy, M., Posamentier, H.W. and Drinkwater, N.J. (2011) Architecture of turbidite channel systems on the continental slope: Patterns and predictions. *Marine and Petroleum Geology*, **28,** 728-743.

Meckel III, L.D., Ibrahim, A.B. and Pelechaty, S.M. (2000) Turbidite Deposition in a Muddy Bypass System on the Upper Slope, Offshore Brunei. In: *AAPG International Conference Abstracts CD (2000)*.

Mellere, D., Plink-Björklund, P. and Steel, R.J. (2002) Anatomy of shelf deltas at the edge of a prograding Eocene shelf margin, Spitsbergen. *Sedimentology*, **49,** 1181-1206.

Morris, E.A., Hodgson, D.M., Brunt, R.L., and Flint, S.S. (2014) Origin, evolution and anatomy of silt-prone submarine external levées. *Sedimentology*, **61**, 1734-1763.

Morton, R.A. and Suter, J.R. (1996) Sequence stratigraphy and composition of Late Quaternary shelf-margin deltas, northern Gulf of Mexico. *American Association of Petroleum Geologists, Bulletin*, **80,** 505-530.

Mountain G.S., Proust J.-N., McInroy D., Cotterill C., and the Expedition 313 Scientists. (2010) Proceedings of the International Ocean Drilling Program, Expedition 313: *Tokyo, Integrated Ocean Drilling Program Management International*.

Mulder, T., Syvitski, J.P.M., Migeon, S., Faugères, J.C. and Savoye, B. (2003) Hyperpycnal turbidity currents: initiation, behavior and related deposits: a review. *Marine and Petroleum Geology*, **20**, 861–882.

Muto, T. and Steel, R.J. (2002) In defense of shelf edge delta development during falling and lowstand of relative sea level. *The Journal of Geology*, **110,** 421-436.

Mutti, E. (1985) Turbidite systems and their relations to depositional sequences. In: *Provenance of Arenites.* (Ed G.G. Zuffa) *NATO-ASI Series, Reidel Publishing Co.*, pp. 65-93.

Mutti, E. and Normark, W.R. (1987) Comparing examples of modern and ancient turbidite systems: Problems and Concepts. In: *Marine Clastic Sedimentology: Concept and case studies* (Eds J.K. Leggett and G.G. Zuffa), pp. 1-38. Graham and Trotman, London.

Mutti, E., Tinterri, R., Benevelli, G., DiBiase, D. and Cavanna, G. (2003) Deltaic, mixed and turbidite sedimentation of ancient foreland basins. *Marine and Petroleum Geology*, **20**, 733–755.

Neal, J. and Abreu, V. (2009) Sequence stratigraphy hierarchy and the accommodation succession method. *Geology*, **37,** 779-782.

Nijman, W. (1998). Cyclicity and basin axis shift in a piggyback basin: towards modelling of the Eocene Tremp-Ager Basin, South Pyrenees, Spain. *Geological Society, London, Special Publications,* **134**, 135-162.

Olariu, C. and Steel, R.J. (2009) Influence of point-source sediment-supply on modern shelf-slope morphology: implications for interpretation of ancient shelf margins. *Basin Research*, **21,** 484-501.

Olariu, M.I., Carvajal, C.R., Olariu, C. and Steel, R.J. (2012) Deltaic process and architectural evolution during cross-shelf transits, Maastrichtian Fox Hills Formation, Washakie Basin, Wyoming. *American Association of Petroleum Geologists, Bulletin*, **96,** 1931-1956.

Oliveira, C.M.M., Hodgson, D.M. and Flint, S.S. (2011) Distribution of soft-sediment deformation structures in clinoform successions of the Permian Ecca Group, Karoo Basin, South Africa. *Sedimentary Geology*, **235**, 314–330.

Owen, G. (2003) Load structures: gravity-driven sediment mobilization in the shallow subsurface. In: *Subsurface Sediment Mobilization* (Eds P. van Rensbergen, R.R. Hillis, A.J. Maltman and C.K. Morley). Geological Society, London, Special Publications, **216**, 21–34.

Payros, A., Tosquella, J., Bernaola, G., Dinarès-Turell, J., Orue-Etxebarria, X., and Pujalte, V. (2009). Filling the North European Early/Middle Eocene (Ypresian/Lutetian) boundary gap: insights from the Pyrenean continental to deep-marine record. *Palaeogeography, Palaeoclimatology, Palaeoecology,* **280**, 313-332.

Patruno, S., Hampson, G.J. and Jackson, C.A.L. (2015) Quantitative characterisation of deltaic and subaqueous clinoforms. *Earth-Science Reviews*, **142,** 79-119.

Petter, A.L. and Steel, R.J. (2006) Hyperpycnal flow variability and slope organization on an Eocene shelf margin, Central Basin, Spitsbergen. *AAPG Bulletin*, **90,** 1451-1472.

Pickering, K.T., Clark, J.D., Ricci Lucchi, F., Smith, R.D.A., Hiscott, R.N. and Kenyon, N.H. (1995) Architectural element analysis of turbidite systems, and selected topical problems for sand-prone deep-water systems. In: *Atlas of Deep Water Environments: Architectural Style in Turbidite Systems* (Eds K.T. Pickering, R.N. Hiscott, N.H. Kenyon, F. Ricci Lucchi and R.D.A. Smith), pp. 1-10. Chapman and Hall, London.

Pickering, K.T., Hodgson, D.M., Platzman, E., Clark, J.D., and Stephens, C. (2001) A new type of bedform produced by backfilling processes in a submarine channel, late Miocene, Tabernas–Sorbas basin, SE Spain. *Journal of Sedimentary Research*, **71**, 692–704.

Plink-Björklund, P. and Steel, R. (2002) Sea-level fall below the shelf edge, without basin-floor fans. *Geology*, **30,** 115-118.

Plink-Björklund, P., and Steel, R. J. (2004) Initiation of turbidity currents: outcrop evidence for Eocene hyperpycnal flow turbidites. *Sedimentary Geology*, **165**, 29-52.

Porębski, S.J. and Steel, R.J. (2003) Shelf-margin deltas: their stratigraphic significance and relation to deepwater sands. *Earth-Science Reviews*, **62,** 283-326.

Porębski, S.J. and Steel, R.J. (2006) Deltas and sea-level change. *Journal of Sedimentary Research*, **76,** 390-403.

Posamentier H.W. and Kolla V. (2003) Seismic geomorphology and stratigraphy of depositional elements in deep-water settings. *Journal of Sedimentary Research*, **73,** 367-388.

Poyatos-Moré, M., Jones, G.D., Brunt, R.L., Hodgson, D.M., Wild, R.J. and Flint, S.S. (2016) Mud-dominated basin-margin progradation: processes and implications. *Journal of Sedimentary Research*, **86,** 863-878.

Prather, B.E. (2000) Calibration and visualization of depositional process models for above-grade slopes: a case study from the Gulf of Mexico. *Marine and Petroleum Geology*, **17,** 619-638.

Prather, B.E. (2003) Controls on reservoir distribution, architecture and stratigraphic trapping in slope settings. *Marine and Petroleum Geology*, **20,** 529-545.

Prather, B.E., Booth, J.R., Steffens, G.S. and Craig, P.A. (1998) Classification, lithologic calibration, and stratigraphic succession of seismic facies of intraslope basins, deep-water Gulf of Mexico. *AAPG Bulletin*, **82,** 701-728.

Prather, B.E., O'Byrne, C., Pirmez, C. and Sylvester, Z. (2016) Sediment partitioning, continental slopes and base-of-slope systems. *Basin Research,* **29**, 394-416.

Pratson, L.F. and Haxby, W.F. (1996) What is the slope of the U.S. continental slope? *Geology*, **24,** 3-6.

Pratson, L.F., Ryan, W.B.F., Mountain, G.S. and Twichell, D.C. (1994) Submarine canyon initiation by downslope-eroding sediment flows: Evidence in late Cenozoic strata on the New Jersey continental slope. *Geological Society of America Bulletin*, **106,** 395-412.

Prélat, A., Hodgson, D.M. and Flint, S.S. (2009) Evolution, architecture and hierarchy of distributary deep-water deposits: a high-resolution outcrop investigation from the Permian Karoo Basin, South Africa. *Sedimentology*, **56**, 2132–2154.

Prélat, A., Pankhania Shyam, S., Jackson, C., A-L. and Hodgson, D.M. (2015) Slope gradient and lithology as controls on the initiation of submarine slope gullies; insights from the North Carnarvon Basin, Offshore NW Australia. *Sedimentary Geology*, **329**, 12-17.

Pyles, D. R., Syvitski, J. P., and Slatt, R. M. (2011). Defining the concept of stratigraphic grade and applying it to stratal (reservoir) architecture and evolution of the slope-to-basin profile: An outcrop perspective. *Marine and Petroleum Geology*, **28**, 675-697.

Ross, W.C., Halliwell, B.A., May, J.A., Watts, D.E. and Syvitski, J.P.M. (1994) Slope readjustment: a new model for the development of submarine fans and aprons. *Geology*, **22,** 511-514.

Ross, W.C., Watts, D.E. and May, J.A. (1995) Insights from Stratigraphic Modeling: Mud-Limited Versus Sand-Limited Depositional Systems. *AAPG Bulletin*, **79,** 231-258.

Rubidge, B.S., Hancox, P.J. and Catuneanu, O. (2000) Sequence analysis of the Ecca—Beaufort contact in the southern Karoo of South Africa. *South African Journal of Geology*, **103**, 81-96.

Ryan, M.C., Helland-Hansen, W., Johannessen, E.P. and Steel, R.J. (2009) Erosional vs. accretionary shelf margins: the influence of margin type on deepwater sedimentation: an example from the Porcupine Basin, offshore western Ireland. *Basin Research*, **21,** 676-703.

Sanchez, C.M., Fulthorpe, C.S. and Steel, R.J. (2012) Miocene shelf-edge deltas and their impact on deepwater slope progradation and morphology, Northwest Shelf of Australia. *Basin Research*, **24,** 683-698.

Scheffler, K., Buehmann, D. and Schwark, L. (2006) Analysis of late Palaeozoic glacial to postglacial sedimentary successions in South Africa by geochemical proxies – Response to climate evolution and sedimentary environment. *Palaeogeography, Palaeoclimatology, Palaeoecology*, **240,** 184-203.

Shepard, F.P. (1972) Submarine canyons. *Earth-Science Reviews*, **8,** 1-12.

Shepard, F.P. (1981) Submarine canyons: multiple causes and long-time persistence. *AAPG Bulletin*, **65,** 1062-1077.

Smith, R.M.H. (1990) A review of stratigraphy and sedimentary environments of the Karoo Basin of South Africa. *Journal of African Earth Sciences (and the Middle East)*, **10,** 117-137.

Spychala, Y.T., Hodgson, D.M., Flint, S.S., and Mountney, N.P. (2015) Constraining the sedimentology and stratigraphy of submarine intraslope lobe deposits using exhumed examples from the Karoo Basin, South Africa. *Sedimentary Geology*, **322**, 67-81.

Steel, R. and Olsen, T. (2002) Clinoforms, clinoform trajectories and deepwater sands. In: *Gulf Coast Section SEPM Foundation, 22nd Annual Research Conference Special Publication, SEPM, CD-ROM.*, pp. 367–381.

Steel, R.J., Porebski, S.J., Plink-Björklund, P., Mellere, D. and Schellpeper, M. (2003) Shelf-edge delta types and their sequence-stratigraphic relationships. In: *Shelf Margin Deltas and Linked Down Slope Petroleum Systems: Global Significance and Future Exploration Potential*, pp. 205-230, Houston, Texas.

Stevenson, C.J., Jackson, C.A.-L., Hodgson, D.M., Hubbard, S.M. and Eggenhuisen, J.T. (2015) Deep-water sediment bypass. *Journal of Sedimentary Research*, **85,** 1058-1081.

Suter, J.R. and Berryhill, H.L. (1985) Late Quaternary shelf-margin deltas, Northwest Gulf of Mexico. *AAPG Bulletin*, **69,** 77-91.

Sydow, J. and Roberts, H.H. (1994) Stratigraphic framework of a late Pleistocene shelf-edge delta, Northeast Gulf of Mexico. *AAPG Bulletin*, **78,** 1276-1312.

Sylvester, Z., Pirmez, C., and Cantelli, A. (2011). A model of submarine channel-levee evolution based on channel trajectories: Implications for stratigraphic architecture. *Marine and Petroleum Geology*, **28**, 716-727.

Sylvester, Z., Deptuck, M.E., Prather, B.E., Pirmez, C. and O'Byrne, C. (2012) Seismic Stratigraphy of a Shelf-Edge Delta and Linked Submarine Channels in the Northeastern Gulf of Mexico. In: *Application of the Principles of Seismic Geomorphology to Continental-Slope and Base-of-Slope Systems: Case Studies from Seafloor and Near-Seafloor Analogues, SEPM Society for Sedimentary*

Geology Special Publication, 99 (Eds B. Prather, M.E. Deptuck, D. Mohrig, B. Van Hoor and R.B. Wynn), pp. 31-59.

Talling, P.J., Masson, D.G., Sumner, E.J. and Malgesini, G. (2012) Subaqueous sediment density flows: depositional processes and deposit types. *Sedimentology*, **59**, 1937-2003.

Tankard, A., Welsink, H., Aukes, P., Newton, R. and Stettler, E. (2009) Tectonic evolution of the Cape and Karoo basins of South Africa. *Marine and Petroleum Geology*, **26,** 1379-1412.

Van Lente, B. (2004) *Chemostratigraphic trends and provenance of the Permian Tanqua and Laingsburg depocentres, South Western Karoo Basin, South Africa. Unpublished Ph.D. thesis*, University of Stellenbosch, South Africa, 339 pp.

Van Wagoner, J.C., Mitchum, R.M., Campion, K.M. and Rahmanian, V.D. (1990) Siliciclastic Sequence Stratigraphy in Well Logs, Cores, and Outcrops: concepts for high-resolution correlation of time and facies. *American Association of Petroleum Geologists, Methods in Exploration Series* **7**, 55 pp.

Veevers, J.J., Cole, D.I. and Cowan, E.J. (1994) Southern Africa: Karoo Basin and Cape Fold Belt. In: *Permian-Triassic Pangean Basins and Foldbelts along the Panthalassan Margin of Gondwanaland: Geological Society America, Memoir* **184** (Eds J.J. Veevers and C.M. Powell), pp. 223-279.

Visser, J.N.J. (1993) Sea-level changes in a back-arc-foreland transition: the late Carboniferous-Permian Karoo Basin of South Africa. *Sedimentary Geology*, **83,** 115-131.

Visser, J.N.J. (1994) A Permian argillaceous syn-to post-glacial foreland sequence in the Karoo Basin, South Africa. *Earth's Glacial Record. International Geological Correlation Project*, **260,** 192-203.

Visser, J.N.J. (1997) Deglaciation sequences in the Permo-Carboniferous Karoo and Kalahari basins of southern Africa: a tool in the analysis of cyclic glaciomarine basin fills. *Sedimentology*, **44,** 507-521.

Walsh, J. P., Alexander, C. R., Gerber, T., Orpin, A. R., and Sumners, B. W. (2007). Demise of a submarine canyon? Evidence for highstand infilling on the Waipaoa River continental margin, New Zealand. *Geophysical Research Letters*, **34,** 20, 1-5.

Walsh, J. P., and Nittrouer, C. A. (2009). Understanding fine-grained river-sediment dispersal on continental margins. *Marine Geology*, **263**, 34-45.

Wickens, H.d.V. (1994) *Basin Floor Fan Building Turbidites of the Southwestern Karoo Basin, Permian Ecca Group, South Africa. Unpublished PhD thesis*, University of Port Elizabeth, Port Elizabeth (South Africa), 233 pp.

Wild, R., Flint, S.S. and Hodgson, D.M. (2009) Stratigraphic evolution of the upper slope and shelf edge in the Karoo Basin, South Africa. *Basin Research*, **21,** 502-527.

Wild, R., Hodgson, D.M. and Flint, S.S. (2005) Architecture and stratigraphic evolution of multiple, vertically-stacked slope channel complexes, Tanqua depocentre, Karoo Basin, South Africa. In: *Submarine Slope Systems: Processes and Products: Geological Society of London, Special Publication* **244** (Eds D.M. Hodgson and S.S. Flint), pp. 89-111.

Wilson, A., Flint, S., Payenberg, T., Tohver, E. and Lanci, L. (2014) Architectural Styles and Sedimentology of the Fluvial Lower Beaufort Group, Karoo Basin, South Africa. *Journal of Sedimentary Research*, **84,** 326-348.

Winker, C.D. and Edwards, M.B.Y. (1983) Unstable Progradational Clastic Shelf Margins. In: *The Shelfbreak* (Eds D.J. Stanley and G.T. Moore). SEPM Special Publication Vol. **33**, pp. 139-157.

Winn, R.D., and Dott, R.H. (1977) Large-scale traction structures in deep-water fan-channel conglomerates in southern Chile. *Geology*, **5**, 41–44.

Zavala, C., Arcuri, M., Di Meglio, M., Gamero, H. and Contreras, C. (2011) A genetic facies tract for the analysis of sustained hyperpycnal flow deposits. In: *Sediment Transfer from Shelf to Deep*

Water – Revisiting the Delivery System (Eds R.M. Slatt and C. Zavala). AAPG Studies in Geology,

61, pp. 1–21.

FIGURE CAPTIONS

Fig. 1. (A) Slope-readjustment model to illustrate how erosional or 'out of grade' margins transform into progradational or 'graded' as an over-steepened margin is healed by onlapping and aggrading deposits. Seismic-reflection examples of clinothems within degradation surfaces (B), channels/valleys/canyons (C), and MTC scours (D) and (E) can be compared in scale and geometry to the Geelhoek dip section. Images modified from Ross *et al*. (1995) (A), offshore New Jersey, USA [(B) IODP Exp. 313, Mountain *et al*., 2010], southern North Sea [(C) and (E) Harding 2015] and offshore Brazil (D).

Fig. 2. (A) South-western Karoo Basin with Tanqua and Laingsburg depocentres outlined. (B) Tanqua depocentre study area. (C) Geelhoek locality; log positions are shown in white, coloured lines represent the tops of parasequences P4, P6, P9 and P10. Images from Google Earth. (D) Summary stratigraphy of the Tanqua depocentre adapted from Wickens (1994), Wild *et al*. (2009) and Flint *et al*. (2011).

Fig. 3. (A) Vertically exaggerated photo-panorama of the arcuate Geelhoek outcrop. Coloured lines are the same as in Fig. 2C, following the tops of P4, P6, P9 and P10. (B) Correlation showing architectural detail of the shelf margin and the large-scale erosion feature. Assuming P10 as a flat datum, tops of P9 and P6 are dipping, and parasequences are thicker towards the centre of the correlation (north and north-east) coinciding with the position of the erosive feature. Blue dotted line represents a regional maximum flooding surface and the red line is an interpreted sequence boundary. (C) Facies map for P4 time. Dotted white line shows the starting point of the soft-sediment deformation in P4 and marks the orientation of the rollover. On rose diagrams, green represents unidirectional palaeocurrents and blue represents bidirectional palaeocurrents.

Fig. 4. (A) Summary log of the Geelhoek succession. (B) Palaeocurrent distribution by parasequences and type of measurement. Note the dominant north/north-west directions from P1 to P4 that change inside the erosive feature to be mainly north-east and revert back to north/north-west again once outside the erosional cut. Within the erosive feature north-east directions in the base pass to more dispersed upward consistent with decreasing confinement. Above P6 palaeocurrents become progressively more dispersed upward. Wave reworking shows a strong north-east/south-west dominance but becomes more north/south in P9 and P10. Current = unidirectional palaeocurrents; Top = bidirectional palaeocurrents measured on symmetrical rippled tops of beds; Parting = parting lineation; Base = sole marking; Gullies = channel or gully orientation; Fold = folding in soft sediment deformation; Wood = orientation of petrified wood fragments at bed bases. (C) Facies percentage comparison between the GH6 proximal position and the GH2 distal position. Note: no deformation or proximal delta front deposits in distal P6; delta plain and a large percentage of delta front deposits in proximal P8 related to no delta plain and a greater proportion of prodelta and deformed deposits in distal P8; distributary channels and delta plain deposits in proximal P9 in contrast to no delta plain or channel deposits and dominant prodelta deposits in distal P9; high proportion of delta plain deposits and no prodelta deposits in proximal P10 related to prodelta deposits still present in distal P10.

Fig. 5. Representative photographs and field sketches of Facies Association A: Structureless and erosive sandstone-dominated deposits.

Fig. 6: Representative photographs and field sketches of Facies Association B: Traction-dominated sandstone/siltstone deposits.

Fig. 7: Representative photographs and field sketches of Facies Association C: Inverse to normal-graded, siltstone-dominated deposits.

Fig. 8. (A) Detailed photo-panorama of the Geelhoek erosive surface, (B) architectural detail interpretation (C) with 50% vertically exaggeration. Logs positions are shown in white. (D) Walked out correlation between GHm and GH6 logs. Note slope turbidites at the base of GH6; shelf-edge distributary channels in P4 in GH6; undeformed to deformed proximal mouth bars towards the centre of the correlation in P4; multiple erosive

surfaces in the proximal areas (GH1 and GH6) passing into paraconformable contacts in GH6 and GHm. Also note the large, deformed block in the canyon margin as part of the initial failure in GH1; and later deposits onlapping it with an angular relationship; the transition from deformed to undeformed deposits at the top of P6 towards the north; the stepped character of the erosive surface between GH1 and GH5 and the steeper northern margin between GH2 and GHm; the channels confined within the erosive feature and deposits onlapping the margins; and that P6 deposits downlap the interpreted maximum flooding surface.

Fig. 9. (A) Outcrop detail of progressive onlap of sedimentary infill over stepped topography and truncation of underlying parasequences; (B) complex geometry with multiple erosive surfaces truncating P4 and P5; and (C) asymmetry of the northern, steeper margin (see Fig. 8 for location).

Fig. 10. Representative photograph of the complete fill of the large-scale erosive feature showing the distinctive fining-upward and thinning-upward stacking pattern (see Fig. 8 for location).

Fig. 11. Basin-margin evolution: (A) aggradation and progradation of P1 to P3; (B) abrupt basinward progradation of P4 over P1 to P3, steepening the margin. Note the change from undeformed to deformed deposits approaching the rollover; (C) progradation of P5 over P4. There is uncertainty as to whether P5 reached the shelf edge; (D) shelf edge degradation, erosion and sequence boundary generation; possible presence of mass-transport deposits basinward; (E) compensational filling that evolves from bypass dominated to deposition dominated; (F) initial healing with progradation of P6 inside the erosive feature, displaying steep clinothems; (G) final healing with deposition of P7 to P10. Not to scale. For legend of colours see Fig.6.

Fig. 12. (A) Palaeogeographic reconstruction of the study area during P4/P5 times, showing significant lateral variability in the shelf-edge and upper-slope morphology. Note the correlation between the incised canyon at Geelhoek, the smaller scale gullies or aprons at Ouberg Pass and their coeval distributary channels eroding proximal mouth bars in the shelf edge at Paardeberg Ridge. 1 and 2: interpreted timing between delta lobes.

(B) Comparison between the study area and the Pleistocene Fuji–Einstein shelf-edge system in the Gulf of Mexico. Note the similar scale when overlaying the trace of the outcrop studied. Modified from Sylvester *et al*. (2012).

Fig. 13. Origin and migration of erosive features. Erosion migrates tens of kilometres northward from Paardeberg to Geelhoek during P4 and P5 times. (1) to (3) Delta lobes migrate towards Geelhoek together with minor gullies generated in the upper slope, showing compensational stacking of delta lobes and erosional features during relative sea level lowering. (4) Period of relative sea level rise. (5) to (7) Progradation over an already sand-rich shelf and shelf edge that increased oversteepening. Subsequent destabilization, bypass and erosion. Channel/gully trapping created a larger conduit in the area. Not to scale.

Table. 1. Facies classification, description and process interpretations. Modified from Gomis-Cartesio *et al.* (2017).

Table. 2. Summary of facies associations: FA-1 – Diffuse laminated to structureless mudstones; FA-2i – Heterolithic siltstone-dominated thin beds; FA-2ii – Heterolithic sandstone-dominated thin beds; FA-3i – Thin to medium-bedded sandstones; FA-3ii – Medium to thick-bedded sandstones; FA-4 – Deformed facies associations. Sd – Sandstone, St – Siltstone, Md – Mudstone.

	Picture	Litho-facies	Sedimentary structures	Thickness, lithology and textural properties	Process interpretation	Others	In FA:
Conglomerate facies (C)		Ci	Matrix to clast-supported intraforma-tional conglomerate, crudely cross-stratified	Centimetre to decimetre-long clasts. Siltstone to sandstone matrix, with mudstone, siltstone or sandstone clasts, 0.5 to 20 cm in diameter. Irregular contacts, common erosive bases and gradational tops	Bedload transport and deposited as basal lag when flow loses energy and is unable to transport coarse grains. Weakly developed cross-bedding indicate migration of dunes and bars. Clasts and debris from bank collapse and erosion	Trough cross-bedding highlighted by sandstone stringers (dark-grey and light-grey beds and subtle change in grain size). Reddening of lags may represent oxidation of iron-rich minerals	FA-3ii
		Cm	Mudstone clast-horizon	Horizons of claystone and siltstone rip-up clasts within fine or medium-grained sandstone beds. Clasts <20 cm, rounded to angular, typically poorly sorted and commonly on erosion surfaces	Mudstone clasts entrained from erosion of underlying claystone and siltstone during scour	Common alignment or imbrication of mudstone clasts	FA-3ii

Sandstone facies (S)	Vertical scale: 50 cm	**Ss**	Structureless	Centimetre to metre-scale poorly to moderately sorted very fine to medium-grained sandstone. Sharp base and top, rarely erosive	'*En masse*' deposition from high-velocity, high-density sediment gravity flows; rapid deposition under upper-flow regime conditions prevented bedform development	Internal structures overprinted by weathering, intensive bioturbation or dewatering. Local abundance of plant remains and oxidized organic matter	FA-2, FA-3, FA-4
		Sg	Inverse or normal grading	Centimetre (to metre)-scale moderately to well-sorted very fine to fine (or medium)-grained sandstone. Base and top can be either sharp or gradational	Normal grading due to waning-flow conditions, inverse grading reflects of waxing-flow conditions likely to be associated with river floods	Plant debris and mica, and development of composite (waxing–waning flow) beds	FA-2, FA-3, FA-4
		Sp	Parallel bedding	Centimetre to metre-scale moderately to well-sorted very fine to fine-grained sandstone. Sharp top and base, rarely erosive or gradational. Common parting lineation	Deposition under upper-phase plane bed conditions. Parting lineations can be produced by turbulent eddies or microvortices at the bed boundary layer. Vertical aggradation under	Parting lineation, mudstone clasts, oxidized organic matter and plant fragments	FA-2, FA-3, FA-4

Vertical scale: 40 cm				shallow-flow conditions	observed in parallel laminae	
Vertical scale: 1 m	Sl	Low angle cross-bedding, SCS or HCS	Centimetre to metre-scale well-sorted very fine to fine-grained sandstone. Sharp base and top, rarely erosive. Common undulatory tops	Large-scale dunes and barforms, deposited under low- flow regime conditions. Deposition in broad bedload sheets affected by combined flows	Well-sorted rounded grains, mudstone clasts on erosive bases and common symmetrical-rippled bedtops	FA-2, FA-3, FA-4
	Sx	High angle planar or trough cross-bedding	Centimetre to metre-scale moderately-sorted very fine to medium-grained sandstone. Sharp base and top, rarely erosive	Planar cross-stratification represents migration of 2D subaqueous dunes. Trough cross-bedding is interpreted to reflect the migration of 3D dunes. 3D dunes occur under lower flow regime conditions and are associated with both downstream and laterally	Mudstone clasts, oxidized organic matter and plant fragments observed on cross-sets	FA-3, FA-4

				accreting barforms		
	Sr	Ripple or climbing ripple-lamination	Millimetre to decimetre-scale moderately-sorted very fine to fine-grained sandstone. Generally sharp or gradational bases and asymmetrical-rippled tops	Tractional features developed under lower flow regime conditions. Asymmetrical current ripples produced by uni-directional flows. Climbing ripples reflect a high sedimentation rate	Locally stoss and lee sides of bedforms preserved	FA-2, FA-3, FA-4
Vertical scale: 40 cm	**Sw**	Wavy lamination and symmetrical ripple-lamination	Millimetre to decimetre-scale well-sorted very fine to fine-grained sandstone. Generally sharp or gradational bases and symmetrical rippled tops	Tractional features developed under lower flow regime conditions, with symmetrical ripple crests due to bi-directional wave motion under orbital currents. Secondary ladder-back ripple sets formed between larger ripple troughs	Well-sorted, rounded grains. Common superimposition of interference ripples	FA-2, FA-3, FA-4

Mudstone facies (M)						
	 Vertical scale: 15 cm	**Ms**	Parallel to ripple-laminated, normally and inversely-graded fissile siltstones and mudstones	Millimetre to decimetre-scale poorly to moderately sorted coarse siltstone beds. Contacts are generally gradational, locally sharp bases	Deposition from very low-density turbidity/hyperpycnal currents, associated with river floods. Post-depositional compaction masks primary sedimentary structures	Starved and lenticular unidirectional ripples	FA-1, FA-2, FA-4
	 Vertical scale: 40 cm	**Md**	Dark grey to black structureless siltstones and mudstones	Millimetre to metre-scale moderately to well-sorted medium to fine siltstone beds. Generally gradational contacts, locally sharp	Hemipelagic fall-out during times of low clastic input	Often associated with sideritic concretion horizons	FA-1, FA-2, (FA-4)

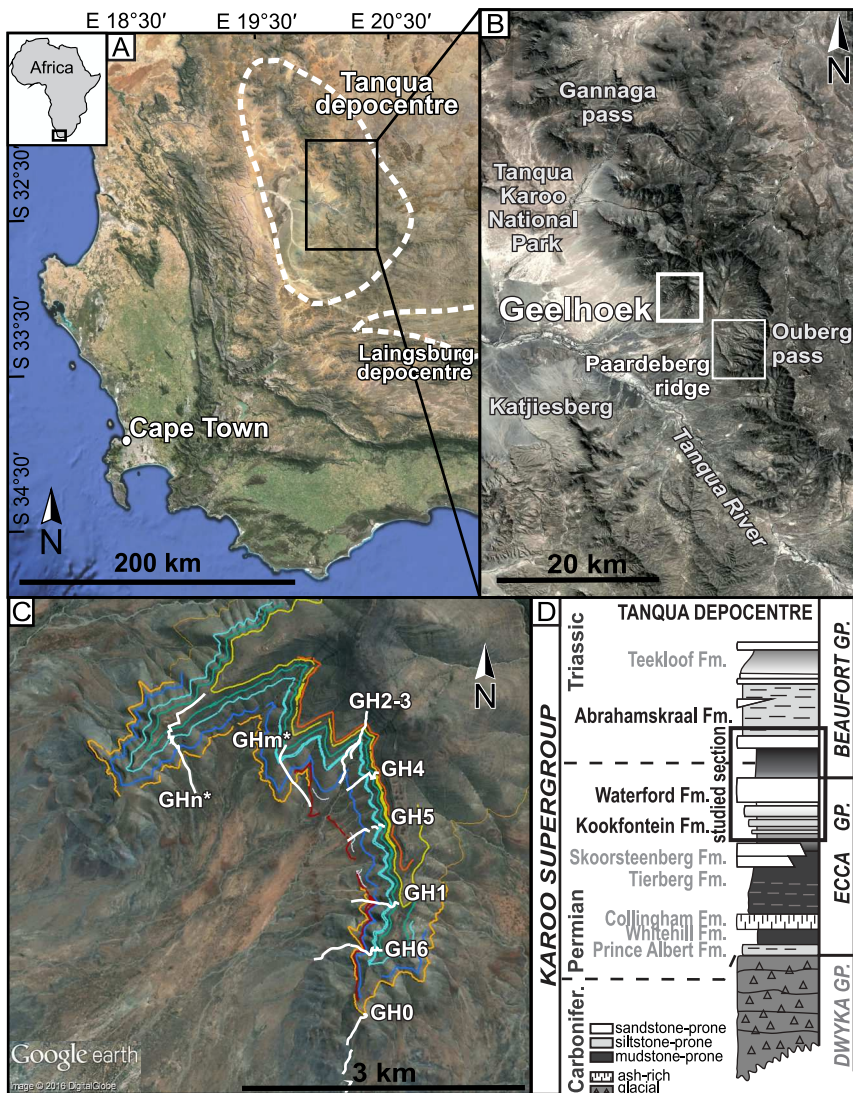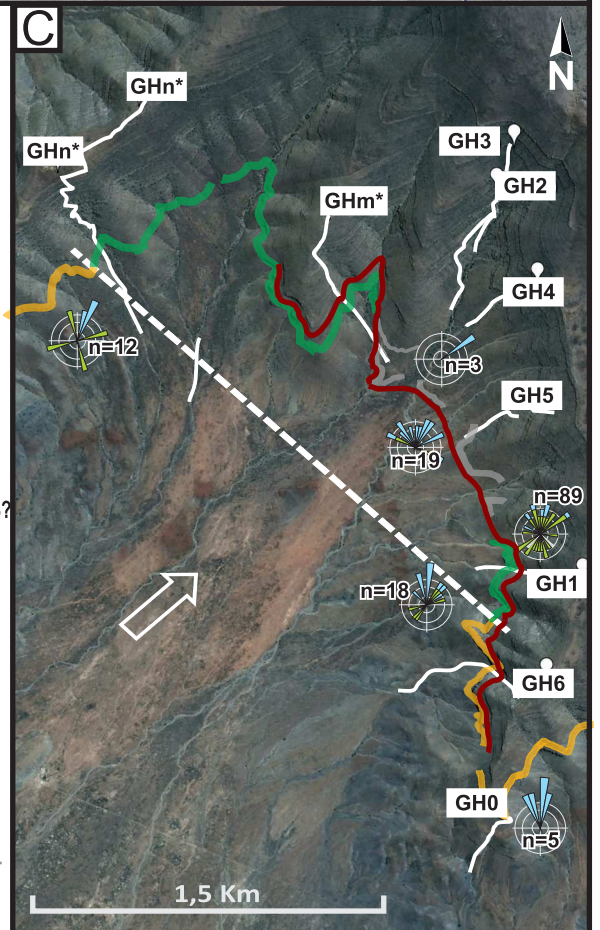|	Mo	Light-grey to olive-green, structureless to well-laminated siltstones and mudstone	Centimetre to metre-scale poorly to moderately sorted coarse to fine siltstone beds. Generally gradational contacts, locally sharp	Deposition by direct fallout from suspension, or debris-flow activity leading to structureless appearance. Green colouration indicates a waterlogged environment. Each sheet represents a separate flooding event from a local breach point. Repeated flooding from similar locations produces bedsets	Local development of carbonate-rich nodular levels	FA-1, (FA-2)

Vertical scale: 1 m

FA-1, (FA-2)
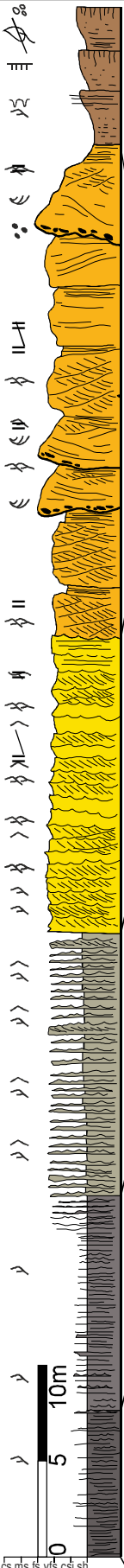
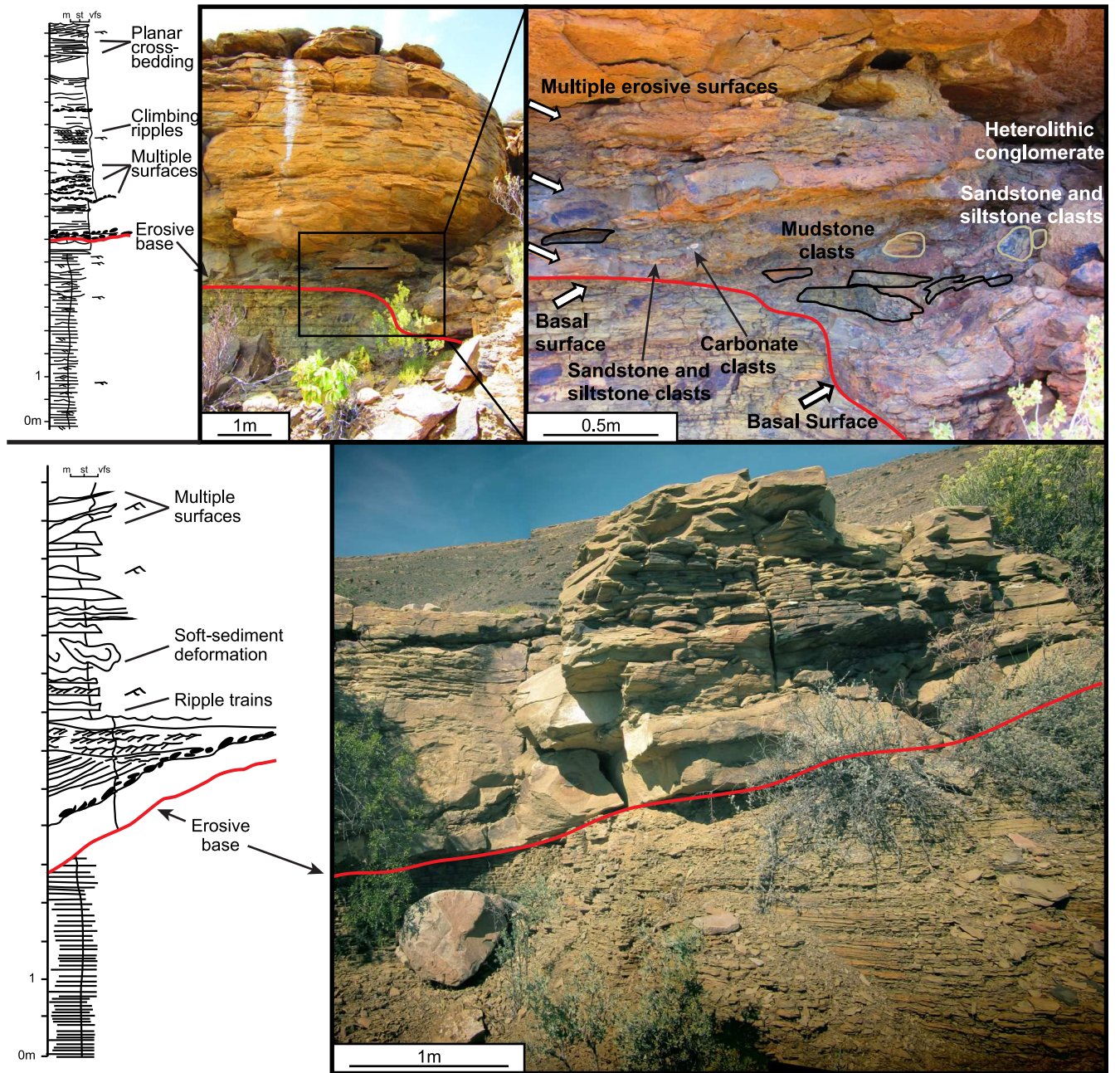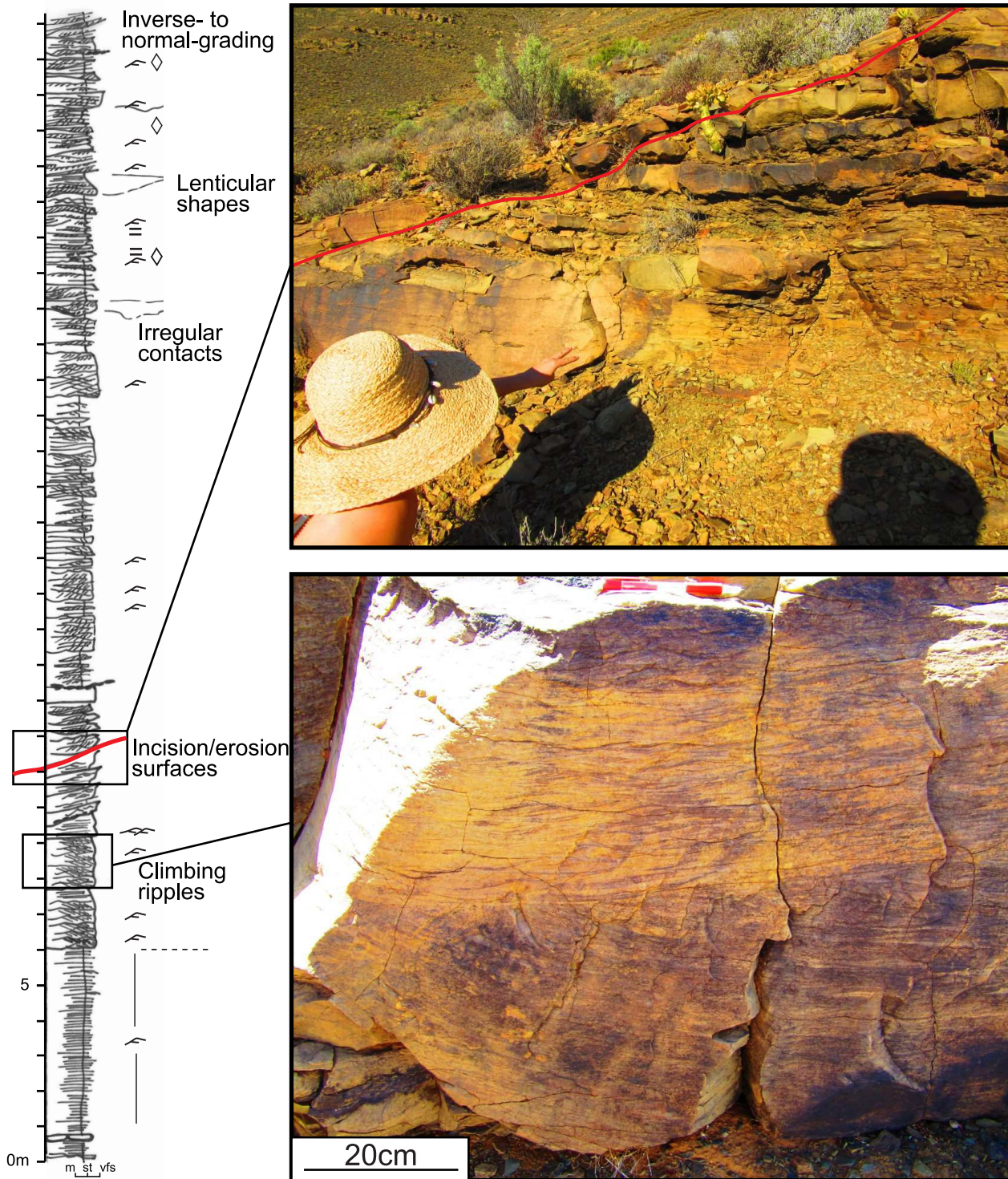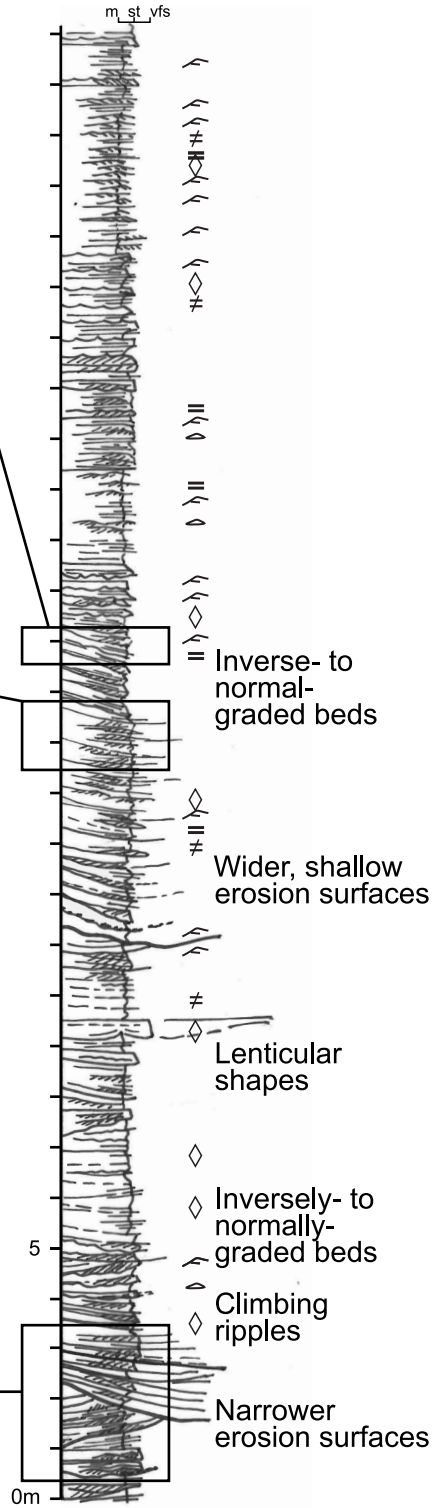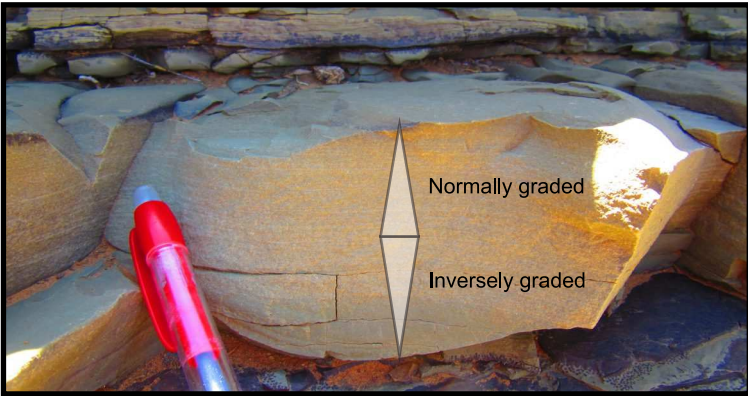| Facies Ass.	Description	Interpretation
FA 4	- Local folded and distorted Sd or St (FA-1, 2, 3). - Soft-sediment deformation: from complete destruction of primary sedimentary structures and disaggregation to coherent upward directed folds in Sd. - <5 m-high dewatering structures.	- in-situ foundering or remobilisation, related to failure or gravitational collapse of oversteepened delta front or channel margin.
FA 3ii	- Laterally extensive or channelised, very fine- to fine-grained predominantly structureless or graded Sd bedsets (Ss, Sg). - Amalgamation surfaces, scattered Md clasts (Cm) and fluid-escape structures. - Transitions between SS, thick-bedded Sp or Sl and Sr-Sw thick-bedded Sd. - Laterally, bedsets onlap directly onto inclined erosional surfaces or pass into thin-bedded Sd (FA-3i) and interbedded Sd and St (FA-2). - Intraformational clast-supported to sandy matrix-supported conglomerate in base of channelized features. - Bioturbation highly variable. - Organic fragments on bedding planes.	- SS, Sg: rapid deposition and frictional freezing from high-density sediment gravity flows. - Basal Md clast horizons are residual lags from bypassing flows. - Sp: Upper phase plane bedding or downstream migration of very low-amplitude long-wavelength bedforms. - Cross- and ripple-laminated beds indicate aggradation and traction processes. -Filling central parts of scours or channels, or upper part of mixed-influenced proximal mouth bars.
FA 3i	- Fine to very fine-Sd beds up to 20 cm-thick, normally or inversely graded (Sg). - Common parallel lamination (Sp), trough cross-bedding or low-angle/hummocky cross-stratification (Sx, Sl) and climbing-ripple cross-lamination (Sr). - Bed tops: symmetrical and asymmetrical ripples on bed tops. - Bioturbation moderate to high. - Organic fragments on bedding planes.	- Normal- and/or inverse-graded beds: river-derived hyperpycnites. - Structured beds: tractional reworking by high concentration flows. - Climbing ripples: high sedimentation rate and abrupt decrease in flow confinement. - Depositional environments: *Planar, trough and climbing-ripple cross-lamination related to unidirectional flows in distal mouth bars. *Low-angle, HCS-SCS in cleaner Sd related to distal wave-influenced delta front or lower shoreface.
FA 2ii	- Laterally-extensive (100's m) <15 m-thick beds. - Thin-bedded (cm) very-fine Sd (Sl, Sg, Sr, Sw) alternating with St (Ms). - Local erosional bed bases and inverse grading in Sd. - In places medium- to thick-beds (<50 cm) of fine-grained Sd (Ss, Sg, Sl) forming lenticular packages. - Bioturbation moderate to high. - Common unclassified organic fragments.	- Deposits of moderate- to low-concentration turbidity currents in both confined (within erosive surfaces) and unconfined settings. - Proximal prodelta or shoreface-offshore transition. - Local thicker sandstone beds: rapidly expanding, energetic turbulent suspension flows.
FA 2i	- Thin- to very thin-bedded (cm-mm), St (Ms) interbedded with very fine Sd (Sr, Sw), showing inverse to normal grading (Sg). - Tabular packages or wedges of slightly inclined strata that drape and/or onlap erosion surfaces. - Bioturbation low to moderate. - Common organic debris.	- Low-concentration turbulent suspension flows distal/lateral to denser hyperpycnal flows; or dilute turbidity currents in unconfined settings. - Distal prodelta/offshore transition but with wave influence.
FA 1	- Structureless fine-medium St (Md, Mo) interbedded with coarse-St beds (Ms). - Parallel lamination, isolated/ starved mm-scale ripples or gently undulating lamination. - Dark-grey to green (light-green to purple). - Bioturbation low to moderate.	- Suspension fallout and dilute turbidity currents below storm wave base on outer shelf or upper slope. - Similar description is found for background deposition in quite/embayed waters of the delta/flood plain (Mo+Ms) but in light-green to purple colours

Table. 2

A

shelf
sea level
slope
base-of-slope

erosional unconformity (slope readjustment surface)

prograding wedge

MTC

delta plain
delta front
prodelta+offshore

onlapping fan/apron deposits

sea level

Aggradation progradation (A-C)
Degradation - bypass (D)
Bypass - filling (E)
Healing clinothems (F)
Healing topsets (G)

studied section

B

M27   M28   M29

Oversteepened shelf edge

Degradation surface

200m
10km

Coarse-grained bottomsets

Miocene New Jersey (USA):
Oversteepening and clinothem degradation

C

A'   A

200ms
2km

Shelf

3km

A'

Submarine fan

Slope

A

Prograding topsets

A'

Degradation surface

Healing clinothems

1km

200ms

Submarine Fan

PGS Cenozoic North Sea (UK):
Incised valley fill by prograding clinothems

D

Eocene Santos Basin (Brazil):
clinothem degradation and MTC emplacement

A'   10km

Degradation surface

MTC

Salt diapir

A

1s
2km

Salt diapir

MTC

MTC

MTC

MTC

A

Healing clinothems

1s

Degradation surface

MTC

PGS   1km

E

B'   A'

A'

B'

10 km

Cenozoic North Sea (UK):
Erosion + MTC development, and clinothem healing

B

A'

A
B'

200ms
1km

Prograding topsets

Healing clinothems

MTC

PGS

Degradation surface

A Summary log (GH6+GH3)

B Palaeocurents

C Facies Associations %

Facies Associations legend:
- Deformed strata
- Delta/coastal plain
- Channels
- Proximal delta front / shoreface
- Distal delta front / shoreface
- Prodelta / SOT
- Sandy turbidites
- Offshore

eroded or not exposed

Symbol legend:
- Carbonate concretions
- Cone-in-cone nodules
- Trough cross-bedding
- Hummocky cross-stratification
- Dish structures
- Flames
- Pseudonodules
- Slumps
- Conglomerates
- Mudstone clasts
- Sole marks
- Current Ripples
- Climbing Ripples
- Wave Ripples
- Starved Ripples
- Root marks
- Wood fragment
- Rooted surface
- **BI** High Bioturbation Index

Inverse- to normal-grading

Lenticular shapes

Irregular contacts

Incision/erosion surfaces

Climbing ripples

5

0m

m st vfs

20cm

Normally graded

Inversely graded

m_st_vfs

Inverse- to normal-graded beds

Wider, shallow erosion surfaces

Lenticular shapes

Inversely- to normally-graded beds

Climbing ripples

Narrower erosion surfaces

5

0m

SW ← → NE N ← → S

A

B
GHm* · GH2 · GH4 · GH5 · GH1 · GH6

C
GHm* · GH2 · GH4 · GH5 · GH1 · GH6
P8 · P7 · P6 · P5 · P4 · P3
500m
vertical scale x2

D
SW ← → NE N ← → S
GHm* · GH2 · GH4 · GH5 · GH1 · GH6
Fig. 10
Fig. 9A-B
Fig. 9C

fs — P8
HST
fs — P7
fs — P6
mfs+SB?
P5
FSST?
fs
P4
mrs
fs — P3
HST
fs — P2
fs — P1

Legend:
- Lower delta plain (FA-3ii)
- Delta front/shoreface (FA-3ii)
- Delta front/shoreface (FA-3i)
- Prodelta/SOT (FA-2ii)
- Prodelta/SOT (FA-2i)
- Offshore / slope turbidites (FA-1)
- Deformed deposits (FA-4)
- Upper slope deposits
- fs Flooding surface
- mfs Max. flooding surface
- mrs Max. regressive surface
- SB Sequence boundary

50 m
0 — km — 1

A

southern margin

P6

onlap geometries

P4

complex surface

100m

B

P6

onlap

P6

deformed block

P5

multiple erosive surfaces

P4

P4

30m

C

northern margin

P6

P5

P4

P6

abrupt truncation

onlap geometries

Bypass to deposition-dominated sedimentary fill

P6

mfs

FA-C

FA-B

FA-A

P4

25m

100m

FA-C: Inverse- to normal-graded, siltstone-dom. deposits
FA-B: Traction-dominated sandstone/siltstone deposits
FA-A: Structureless and erosive, sandstone-dominated deposits

A- AGGRADATION + PROGRADATION

B- PROGRADATION (FORCED REGRESSION?)

C- PROGRADATION (AFTER FLOODING?)

D- DEGRADATION + BYPASS

E- BYPASS + FILLING

F- HEALING

G- HEALING

Aprox scale: 700m

Aprox scale: 5km

A

Geehoek
(this study)

Ouberg

Paardeberg
(Gomis et al., 2016)

N

5 km

B

SLOPE

Channel
head

Geelhoek
(this study)

shelf edge

Delta lobe
front

SHELF

Superimposed
outcrop belt

Ouberg

Paardeberg
(Gomis et al., 2016)

5 km

PARASEQUENCE 4

Paardeberg Geelhoek

shelf

SERZ

upper slope

flooded shelf

1 2 3 4

PARASEQUENCE 5

5 6 7

Sandy deltaic lobe

Deformed sediments

Prodelta/slope thin beds

Distributary channels

Active gulley/canyon

Abandoned/filled gulley

Sand-rich turbidites

Mass-transport deposits

Gravitational collapse